Geological Magazine

www.cambridge.org/geo

Petrogenesis and tectonic implications of the early Mesozoic granitoids in the northern Alxa region, Central Asian Orogenic Belt

Xiaochen Zhao[1], Chiyang Liu[2], Jianqiang Wang[2], Yazhuo Niu[3], Lei Huang[2], Shaohua Zhang[4], Fangpeng Du[1], Heng Peng[2], Yingtao Chen[1], Tao Peng[1] and Zhengzheng Mao[1]

[1]College of Geology and Environment, Xi'an University of Science and Technology, Xi'an 710054, China; [2]State Key Laboratory of Continental Dynamics, Department of Geology, Northwest University, Xi'an 710069, China; [3]Key Laboratory for the Study of Focused Magmatism and Giant Ore Deposits, Xi'an Centre of Geological Survey (Northwest China Centre of Geoscience Innovation), China Geological Survey, Xi'an, 710054, China and [4]Shaanxi Key Laboratory of Petroleum Accumulation Geology, School of Earth Sciences and Engineering, Xi'an Shiyou University, Xi'an, 710065, China

Original Article

Cite this article: Zhao X, Liu C, Wang J, Niu Y, Huang L, Zhang S, Du F, Peng H, Chen Y, Peng T, and Mao Z (2023) Petrogenesis and tectonic implications of the early Mesozoic granitoids in the northern Alxa region, Central Asian Orogenic Belt. *Geological Magazine* **160**: 601–622. https://doi.org/10.1017/S0016756822001157

Received: 30 May 2021
Revised: 13 October 2022
Accepted: 18 October 2022
First published online: 21 December 2022

Keywords:
geochemistry; U–Pb geochronology; Hf isotopic composition; granitoids; northern Alxa region; Central Asian Orogenic Belt

Authors for correspondence:
Jianqiang Wang, Email: wjq@nwu.edu.cn;
Xiaochen Zhao, Email: zxcnwu@126.com

Abstract

The northern Alxa region is located in the central segment of the southern Central Asian Orogenic Belt. Many controversies and deficiencies still exist regarding the magma source characteristics, petrogenesis and tectonic regimes during the late Palaeozoic – early Mesozoic period within this region. This study presents whole-rock compositions and zircon U–Pb and Lu–Hf isotopic data for three early Mesozoic I- and A-type granitic plutons occurring in the northern Alxa region. The Haerchaoenji and Chahanhada I-type granitoids yielded zircon $^{206}Pb–^{238}U$ ages of 245 ± 5 Ma and 245 ± 2 Ma, respectively. The variable positive zircon $\epsilon_{Hf}(t)$ values between +1.8 and +11.8, with young T_{DM} ages of 425–837 Ma, indicate that these I-type granitoids were mainly derived from juvenile crustal materials. The Wulantaolegai pluton has a zircon $^{206}Pb–^{238}U$ age of 237 ± 2 Ma and is classified as having high-K calc-alkaline A-type affinity. Furthermore, the positive zircon $\epsilon_{Hf}(t)$ values of the Wulantaolegai granite range from +3.3 to +8.7 with young T_{DM} ages of 545–778 Ma, suggesting the involvement of a juvenile crustal source as well. Furthermore, the major-element compositions of the Chahanhada and Wulantaolegai granites suggest the input of metasedimentary components. Geochemically, the Haerchaoenji and Chahanhada I-type granitoids show an arc affinity, while the Wulantaolegai granite exhibits a post-collisional affinity. However, with regional data, we suggest that the Haerchaoenji and Chahanhada I-type granitoids were also emplaced in a post-collisional setting, and the arc affinity was probably inherited from recycled subduction-related materials. These lines of evidence obtained in this study enable us to argue that the Palaeo-Asian Ocean in the central segment of the Central Asian Orogenic Belt closed before Middle Triassic time.

1. Introduction

The Central Asian Orogenic Belt (CAOB), which is located in northcentral Asia from the Uralides to the Pacific Ocean (e.g. Şengör *et al.* 1993; Jahn *et al.* 2004; Windley *et al.* 2007; Li *et al.* 2013; Xiao *et al.* 2015; Liu *et al.* 2016) (Fig. 1a), has been regarded as one of the world's largest and most complex accretionary orogens (Şengör *et al.* 1993; Windley *et al.* 2007; Xiao *et al.* 2009; Wilhem *et al.* 2012). The CAOB has been widely considered to have undergone long-lived, giant orogenic processes driven by the evolution and closure of the Palaeo-Asian Ocean (PAO) during the Neoproterozoic to Mesozoic period (Şengör *et al.* 1993; Jahn *et al.* 2004; Cope *et al.* 2005; Windley *et al.* 2007; Shen *et al.* 2009; Zhang *et al.* 2009; Cai *et al.* 2011*a*,*b*; Li *et al.* 2013, 2016*a*,*b*, 2017; Xu *et al.* 2013; Xiao *et al.* 2013, 2015; Wang *et al.* 2017; He *et al.* 2018; Song *et al.* 2018*a*,*b*; Chen *et al.* 2019; Zhao *et al.* 2020).

Numerous studies have focused on the multi-stage evolution of the PAO and CAOB, with significant progress made (e.g. Şengör *et al.* 1993; Windley *et al.* 2007; Xiao *et al.* 2009, 2015; Wilhem *et al.* 2012; Eizenhöfer *et al.* 2014; Eizenhöfer & Zhao, 2018). However, the timing of the final closure of the PAO is still debated, with estimates ranging from Late Devonian to Triassic time (e.g. Charvet *et al.* 2011; Xu *et al.* 2013; Eizenhöfer *et al.* 2014, 2015*a*,*b*; Xiao *et al.* 2015, 2018; Zhang *et al.* 2015*a*,*b*; Zhang, W. *et al.* 2015; Shi, G. Z. *et al.* 2016; Yin *et al.* 2016; Song *et al.* 2018*b*). These controversies are mainly due to: (1) the various objects studied, such as the late Palaeozoic magmatic rocks (e.g. Shi *et al.* 2012, 2014*a*,*b*; Xiao *et al.* 2015; Liu *et al.* 2017, 2018; Song *et al.* 2018*a*), tectonic deformation and regional unconformity (e.g. Tang, 1990; Xu *et al.*

© The Author(s), 2022. Published by Cambridge University Press.

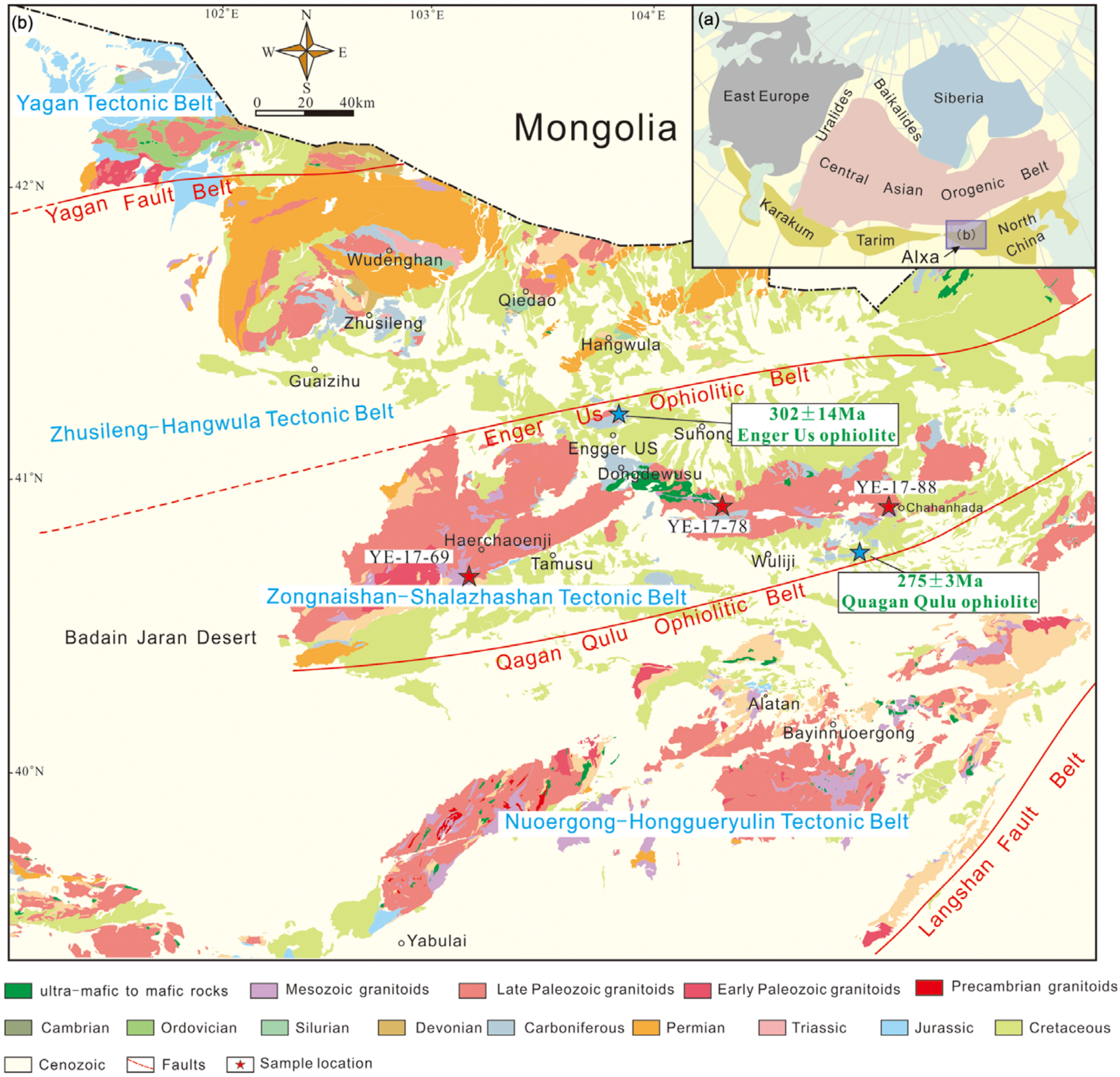

Fig. 1. (Colour online) (a) Schematic geological map of the Central Asian Orogenic Belt (modified after Liu *et al.* 2017). (b) Geological map of the northern Alxa region (modified after 1:200 000 geological maps from BGMRIM, 1991).

2013; Xu, X. Y. *et al.* 2014), or detrital zircon indicators (e.g. Chen *et al.* 2019; Song *et al.* 2018*b*, 2021; Niu *et al.* 2021); (2) limited study areas (different segments probably closed at diverse times); and (3) relatively poor study in some areas because of execrable natural conditions, e.g. the northern Alxa region. Actually, the CAOB evolved with multiple convergences and the accretion of many orogenic components during multiple phases of amalgamation (Xiao *et al.* 2015), i.e. the closure of the PAO was probably diachronous. Furthermore, previous studies of magmatic rocks mainly focused on the Tianshan–Beishan in the western segment (e.g. Yang *et al.* 2014; Zhang, W. *et al.* 2015; Tian *et al.* 2017) or Inner Mongolia in the eastern segment (e.g. Jian *et al.* 2008, 2010; Chen *et al.* 2009; Xu *et al.* 2013; Li *et al.* 2016*a*,*b*, 2017; Shi, Y. R. *et al.* 2016; Zhao, P. *et al.* 2017) along the southern CAOB. Much less is known, however, about the central segment of the southern CAOB (the northern Alxa region), which is a crucial junction between the North China Block (NCB) and the Tarim Block (Fig. 1a). It has hampered us from better understanding the evolutionary history of the PAO and subsequent development of the CAOB. In the central segment of the southern CAOB, the late Palaeozoic magmatic rocks are widely exposed and have attracted the attention of many scholars (e.g. Shi *et al.* 2014*a*,*b*; Zhang *et al.* 2017; Liu *et al.* 2017, 2018; Song *et al.* 2018*a*; Zhao *et al.* 2020). Nevertheless, the timing of tectono-magmatic switching from an arc-related to a post-collisional process is still actively debated. Previous research indicated that this region was in a subduction

https://doi.org/10.1017/S0016756822001157 Published online by Cambridge University Press

setting during most of the late Palaeozoic period (e.g. Shi *et al.* 2014*a*,*b*; Zhang *et al.* 2017; Liu *et al.* 2017, 2018; Song *et al.* 2018*a*; Zhao *et al.* 2020). Therefore, the earliest Mesozoic should be a key period in the evolution of the PAO and probably provides significant information to constrain the tectonic switch from a subduction setting to a post-collisional setting.

Thus, this research focused on the earliest Mesozoic magmatic rocks, which have been rarely reported, exposed in the northern Alxa region of the central segment of the southern CAOB. We report new geochronological, geochemical and isotopic data from three early Mesozoic granitoids in the northern Alxa region and evaluate their petrogenesis and tectonic implications, in order to decipher the evolution of the central segment of the southern CAOB.

2. Geological background

The northern Alxa region is situated in western Inner Mongolia, which borders the NCB to the east separated by the Zunnbayan fault belt and the Langshan fault belt (Fig. 1a) (Huang *et al.* 1999; Geng & Zhou, 2010; Zhang *et al.* 2013), and the North Qilian Orogen to the southwest separated by the Longshoushan fault belt (Liu *et al.* 2017). Largely covered by the Badain Jaran desert, the Alxa Block exposes sporadic Precambrian rocks, Palaeozoic to Mesozoic volcanic and intrusive rocks, and Phanerozoic sedimentary rocks. The Alxa Block is generally considered to be a Precambrian block belonging to the westernmost part of the NCB at present (Fig. 1a). Based on palaeontology, sedimentary sequences and magmatic events, some researchers have argued that the northern Alxa region comprised a complete trench–arc–basin system during late Palaeozoic time (Wang *et al.* 1994; Zhang *et al.* 2013). In this region, there are two significant ophiolite belts, i.e. the Qagan Qulu Ophiolite Belt and the Enger Us Ophiolite Belt (Fig. 1b). The Enger Us Ophiolite Belt (~302 Ma) is regarded as the major suture of the PAO in the northern Alxa region (BGMRIM, 1991; Wang *et al.* 1994; Wu *et al.* 1998; Xie *et al.* 2014; Zheng *et al.* 2014), and the Qagan Qulu Ophiolite Belt (~275 Ma) is considered to have been generated in a back-arc setting (Wu *et al.* 1998; Zheng *et al.* 2014). Based on these two sutures and the Yagan fault belt, the northern Alxa region can be further subdivided into four units (from north to south): the Yagan Tectonic Belt (YTB), the Zhusileng–Hangwula Tectonic Belt (ZHTB), the Zongnaishan–Shalazhashan Tectonic Belt (ZSTB) and the Nuoergong–Honggueryulin Tectonic Belt (NHTB) (Wu & He, 1992, 1993) (Fig. 1b).

The ZSTB extends southwestward to the Badain Jaran desert and northeastward to the south of the Solonker region in a nearly ENE–WSW direction (Fig. 1b). To the south, the ZSTB borders the NHTB separated by the Qagan Qulu Ophiolite Belt. Northward, the Enger Us fault separates the ZSTB from the ZHTB. Palaeozoic–early Mesozoic plutons are widely exposed in the ZSTB, including voluminous calc-alkaline granitoids and minor gabbro–diorites (e.g. Shi, G. Z. *et al.* 2016). The geochemical characteristics show that the late Palaeozoic plutonic rocks were mainly involved in the subduction process of the PAO (e.g. Wang *et al.* 1994; Shi *et al.* 2014*a*,*b*). The early Mesozoic plutonic rocks are mainly medium–fine-grained monzogranite and K-feldspar granite, which intruded into the pre-Mesozoic rocks as small stocks or branches (Wang *et al.* 1994). Minor Precambrian rocks are also exposed in the ZSTB, which are mainly composed of metamorphosed supracrustal rocks and meta-intrusive rocks with an age of 1.4~1.5 Ga (Shi, X. J. *et al.* 2016). The lower Palaeozoic sedimentary rocks are absent, while the upper Palaeozoic sedimentary rocks are more prevalent, represented by the upper Carboniferous – lower Permian Amushan Formation (BGMRIM, 1991; Bu *et al.* 2012; Lu *et al.* 2012; Zheng *et al.* 2014; Zhang & Zhang, 2016). The lithology of the lower and middle sections of the Amushan Formation is obviously different from that of the upper section, suggesting a significant tectonic event occurred (Shi *et al.* 2014*a*; Liu *et al.* 2017). The Jurassic sequences are sporadically exposed, which are composed of coarse-grained clastic rocks. By contrast, the Cretaceous sequences are more developed, characterized by volcaniclastic rocks.

3. Field observations and sampling

3.a. Field observations

In the ZSTB, the late Palaeozoic – Early Triassic intrusive rocks constitute the principal part of the Zongnaishan–Shalazhashan Mountain (NXBG, 1980*a*,*b*, 1982, 2001; Zhang *et al.* 2013; Xie *et al.* 2021). The majority of the Triassic intrusive rocks in this region are controlled by E–W or NW-directed faults and are emplaced into the late Palaeozoic granitoids (Fig. 1b) (NXBG, 1980*a*,*b*, 1982, 2001). Furthermore, these Triassic plutons are mainly exposed as small-scale stocks or branches, and mainly consist of granite, monzogranite and granodiorite (NXBG, 1980*a*,*b*, 1982; Zhang *et al.* 2013; Shi *et al.* 2014*a*; Zhang, Z. P. *et al.* 2016; Zhao, Z. L. *et al.* 2016). In this study, we conducted detailed studies on three plutons (the Haerchaoenji, Wulantaolegai and Chahanhada plutons) in the ZSTB. Mafic enclaves associated with these plutons were not observed during the field studies. The locations of the investigated plutons are shown in Figures 1 and 2.

The Haerchaoenji pluton is the largest pluton in the southwestern Zongnaishan area with an outcrop area of ~100 km^2 (NXBG, 1982). The shape of this pluton is complex, and it is mainly exposed as branches and dykes. The strike of this pluton is mostly near N–S, implying that the rock mass intruded along a N–S-directed fault (Yebuerhai Fault) (NXBG, 1982). This pluton intruded the Precambrian gneiss and the Palaeozoic granitoids, and is unconformably covered by the Middle Jurassic strata in the south (Fig. 2a) (NXBG, 1982). The Haerchaoenji pluton is dominated by medium–fine-grained granite, biotite granite and granodiorite (NXBG, 1982). The Wulantaolegai pluton intruded into the upper Carboniferous strata (Fig. 2b) and is dominated by medium-grained granite and monzonitic granite (NXBG, 1980*a*, 2001). The Wulantaolegai pluton is exposed as a rock branch. The Chahanhada pluton is located in the eastern Shalazhashan area, and trends in a NE–SW direction with an outcrop area of ~12 km^2 (NXBG, 1980*b*). This pluton is in the form of an elliptical stock and intrudes the late Palaeozoic granitoids (Fig. 2b). The Chahanhada pluton is unconformably covered by Lower Cretaceous strata (Bayingebi Fm) in the south and east areas (Fig. 2b) (NXBG, 1982). The main rock types are granite and monzonitic granite with a medium to coarse-grained granitic texture (Fig. 3g).

3.b. Sampling

A total of 16 samples were collected from the Haerchaoenji, Wulantaolegai and Chahanhada plutons for systematic zircon U–Pb–Hf isotopic and whole-rock geochemical analysis. The detailed description of these samples is carried out below.

The samples (YE-17-69, 69-1, 69-2, 69-3, 69-4) from the Haerchaoenji pluton are light grey, homogeneous, undeformed

https://doi.org/10.1017/S0016756822001157 Published online by Cambridge University Press

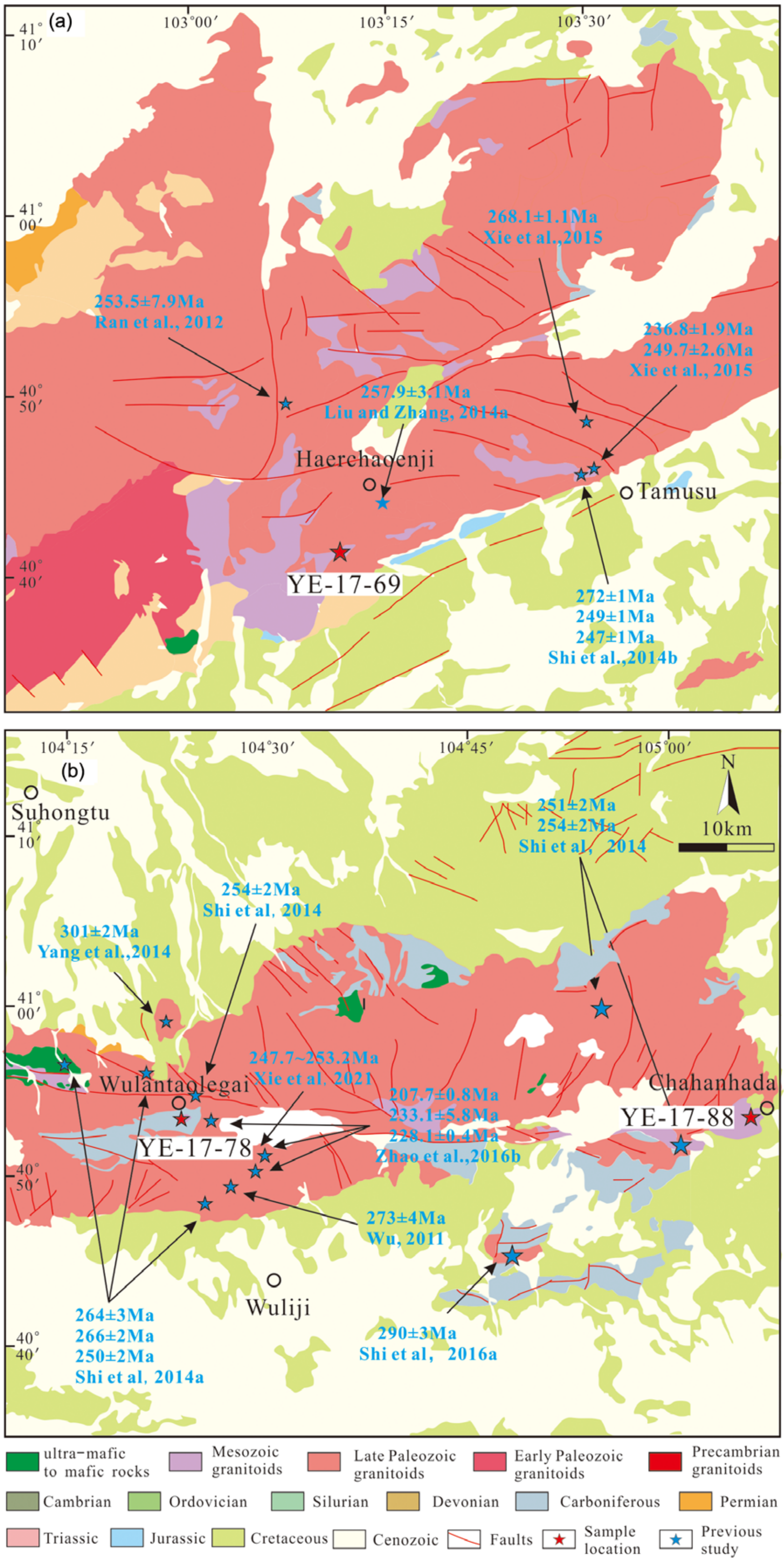

Fig. 2. (Colour online) Geological map of the (a) Zongnaishan and (b) Shalazhashan areas.

https://doi.org/10.1017/S0016756822001157 Published online by Cambridge University Press

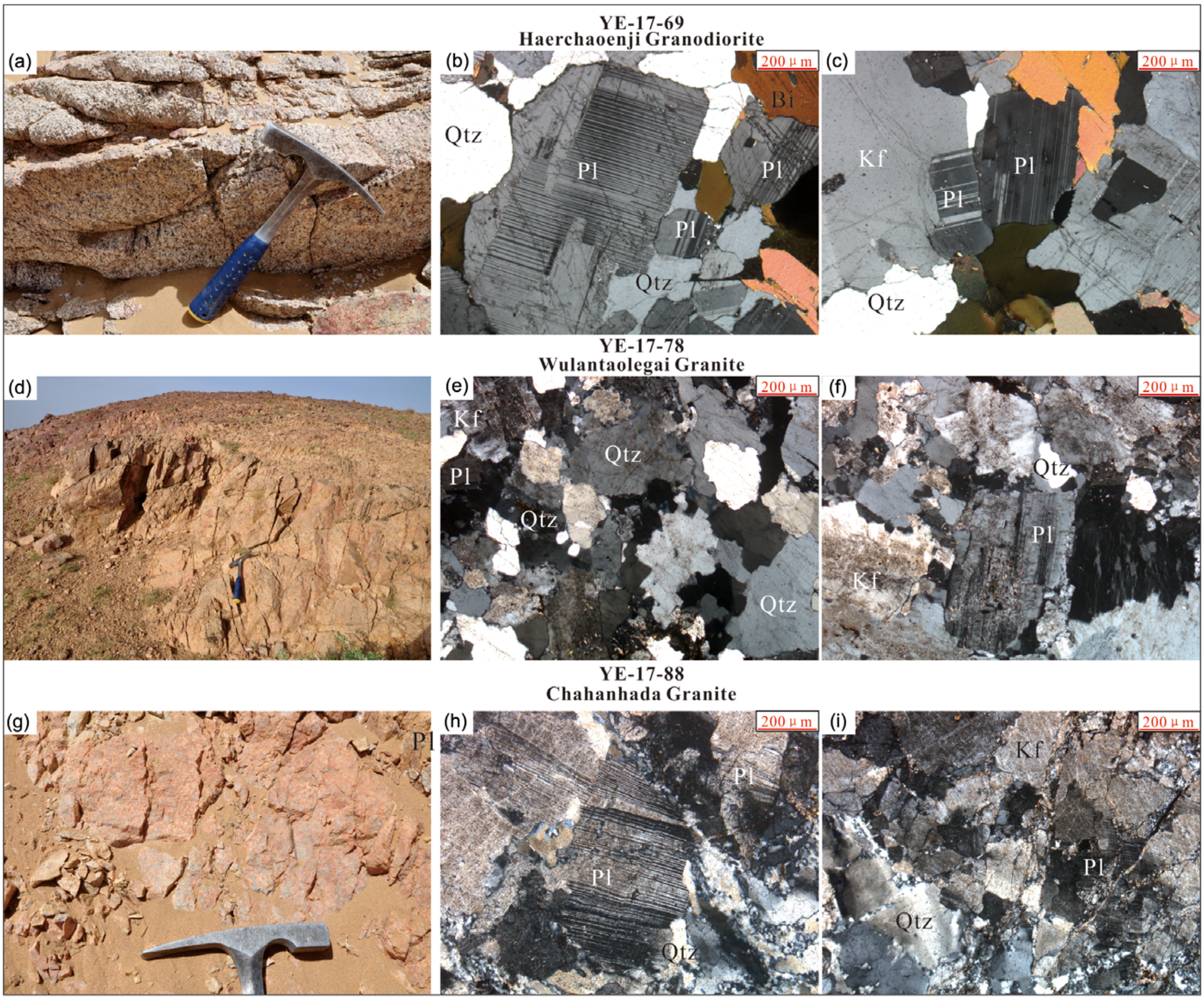

Fig. 3. (Colour online) Field photographs and photomicrographs showing petrographic features of the studied samples. (a–c) YE-17-69; (d–f) YE-17-78; (g–i) YE-17-88. Mineral abbreviations: Pl – plagioclase; Qtz – quartz; Kf-K – feldspar; Bt – biotite. Length of hammer for scale is 290 mm; length of hammer head for scale is 175 mm.

medium-grained granodiorites (3–5 mm) (Fig. 3a). The major mineral assemblages are quartz (~25 vol. %), plagioclase (~45–55 vol. %), K-feldspar (~10–15 vol. %) and biotite (~5–10 vol. %) (Fig. 3b, c), while the main accessory minerals are zircon, apatite and titanite. The plagioclases are subhedral–euhedral and show polysynthetic twinning (Fig. 3b). Most of the K-feldspars are subhedral to anhedral and show features of alteration on their surfaces (Fig. 3c). Some quartz crystals exhibit an anhedral granular texture among other minerals with wavy extinction, indicating dynamic recrystallization (Fig. 3c). Sub- to anhedral biotite is characterized by strong pleochroism, and it occasionally appears as mineral aggregates.

The samples (YE-17-78, 78-1, 78-2, 78-3, 78-4) from the Wulantaolegai pluton are pale red, fine–medium-grained granite (Fig. 3d), primarily composed of K-feldspar (~30–35 vol. %), quartz (~35 vol. %) and plagioclase (20–25 vol. %), with minor biotite (~3 vol. %) (Fig. 3e, f) and accessory minerals (e.g. zircon, magnetite, titanite and apatite). K-feldspars are euhedral or subhedral and show relatively strong alteration. In addition, some K-feldspars show the distinctive feature of gridiron twinning. Quartz crystals are anhedral with rounded borders, while plagioclases are euhedral with polysynthetic twinning (Fig. 3e, f).

The samples (YE-17-88, 88-1, 88-2, 88-3, 88-4, 88-5) from the Chahanhada pluton are pale red, homogeneous medium-grained (3–5 mm) granites (Fig. 3g). Quartz (~35–40 vol. %), K-feldspar (~35–40 vol. %), plagioclase (~20–27 vol. %) and biotite (~1–2 vol. %) (Fig. 3h, i) are the major minerals. Zircon, apatite and titanite are the main accessory minerals. The K-feldspars show obvious evidence of alteration. The plagioclases are zoned with idiomorphic plates and show polysynthetic twinning. The quartz grains exhibit an anhedral granular texture among other minerals and have wavy extinction (Fig. 3h, i).

4. Analytical methods

4.a. Whole-rock major and trace elements

Whole-rock major and trace elements of the studied samples were analysed at the State Key Laboratory of Continental Dynamics, Northwest University, China. Fresh chips of whole-rock samples were powdered to ~200 mesh using a tungsten carbide ball mill. Major elements were analysed using a Rigaku RIX 2100 X-ray fluorescence (XRF) spectrometer, and trace elements were analysed by an Agilent 7500a inductively coupled plasma mass spectrometer (ICP-MS) using United States Geological Survey (USGS) and international rock standards (BHVO-2, AGV-2, BCR-2 and GSP-1). For the trace-element analysis, sample powders were digested using an $HF + HNO_3$ mixture in high-pressure Teflon bombs at 190 °C for 48 hours. The analytical precision and accuracy for most of the major and trace elements is better than 5 % and 10 %, respectively (Liu *et al.* 2007).

4.b. Zircon Lu–Hf isotopic analyses

In situ zircon Hf isotope analysis was undertaken on a Nu Plasma HR multi-collector ICP-MS (Nu Instrument Ltd, UK) equipped with a GeoLas 2005 193 nm ArF excimer laser-ablation system. Analysis was carried out using a beam size of 44 μm and helium was used as a carrier gas. The laser repetition rate was 10 Hz and the energy density applied was 15–20 J cm^{-2}. Instrumental conditions and data acquisition methods were described by Zhao, Y. *et al.* (2017). Time-dependent drifts of Lu–Hf isotopic ratios were corrected using a linear interpolation according to the variations of 91500 and GJ-1. A decay constant of 1.867×10^{-11} a^{-1} for ^{176}Lu (Albarède *et al.* 2006) and the present chondritic ratios of $^{176}Hf/^{177}Hf = 0.282772$ and $^{176}Lu/^{177}Hf = 0.0332$ (Blichert-Toft & Albarède, 1997) were adopted to calculate $\epsilon_{Hf}(t)$ values ($\epsilon_{Hf}(t) = ((^{176}Hf/^{177}Hf)_s - (^{176}Lu/^{177}Hf)_s \times (e^{\lambda t} - 1))/((^{176}Hf/^{177}Hf)_{CHUR,0} - (^{176}Lu/^{177}Hf)_{CHUR} \times (e^{\lambda t} - 1)) - 1) \times 10\,000$; Wu *et al.* 2007). Bea *et al.* (2018) proposed that the best strategy to calculate the Hf T_{DM} is to use the analytically determined whole-rock Lu/Hf ratio as a proxy for the source Lu/Hf. In this study, we use the analytically determined whole-rock Lu/Hf ratio as described by Bea *et al.* (2018).

4.c. Zircon U–Pb geochronology

Zircon grains for U–Pb dating were extracted by using a combined technique of heavy liquid and magnetic separation, and then handpicked under a microscope, mounted in epoxy resin and polished until the centres of the zircon grains were exposed. Cathodoluminescence (CL) images were taken to reveal their internal structures and select the suitable U–Pb dating spots by using a Quanta 400FEG environmental scanning electron microscope.

Laser-ablation ICP-MS (LA-ICP-MS) zircon U–Pb dating was carried out at the State Key Laboratory of Continental Dynamics, Northwest University, China. The U–Pb dating was conducted on an Agilent 7500a ICP-MS instrument equipped with a 193 nm ArF excimer laser and a homogenizing imaging optical system. A fixed spot size of 32 μm with a laser repetition rate of 6 Hz was adopted throughout this study. Helium was used as carrier gas to provide efficient aerosol delivery to the torch. The standard silicate glass NIST 610 was used to optimize the instrument to obtain maximum signal intensity (^{238}U signal intensity >460 cps/ppm) and low oxide production (ThO/Th <1 %). The ICP-MS measurements were carried out using time-resolved analysis operating in fast peak jumping mode and DUAL detector mode using a short integration time. $^{207}Pb/^{206}Pb$, $^{206}Pb/^{238}U$, $^{207}Pb/^{235}U$ and $^{208}Pb/^{232}Th$ ratios were calculated using the GLITTER 4.0 program (Macquarie University). The zircon 91500 was used as an external standard with a recommended $^{206}Pb–^{238}U$ age of 1065.4 ± 0.6 Ma (Wiedenbeck *et al.* 1995) for correction of both instrumental mass bias and depth-dependent elemental and isotopic fractionation. U, Th and Pb concentrations were calibrated by using ^{29}Si as an internal standard and NIST SRM 610 as an external standard. Concordia diagrams and weighted mean calculations were made using the Isoplot program (version 3.0) (Ludwig, 2003).

5. Analytical results

5.a. Whole-rock geochemistry

In this research, field investigation and photomicrographs reveal that these intermediate–acid intrusive rocks have rarely been affected by regional metamorphism. Major- and trace-element compositions of selected granitoids from the study area are listed in online Supplementary Material Table S1.

The samples from the Haerchaoenji granodiorite have $SiO_2 = 63.10–65.80$ wt %, total $Fe_2O_3 = 3.86–4.65$ wt %, $Na_2O = 4.52–4.77$ wt %, $K_2O = 1.94–2.15$ wt %, MgO = 1.55–1.91 wt %, Mg no. = 48–49 and CaO = 3.78–4.14 wt % (online Supplementary Material Table S1). In the plot of total alkalis versus SiO_2, these samples all fall into the subalkaline series field (Fig. 4a). In the plot of K_2O versus SiO_2, all samples fall into the medium-K calc-alkaline field (Fig. 4b). These granodiorites collected from the Haerchaoenji pluton are metaluminous to slightly peraluminous, with A/CNK (molecular ratio of $Al_2O_3/(CaO + Na_2O + K_2O)$) ratios ranging from 0.97 to 1.01 (Fig. 4c). In addition, these samples show enrichment of light rare earth elements (LREEs) ($(La/Yb)_N = 27.13–41.31$) and no obvious Eu anomalies (Eu = 0.95–1.02) in the chondrite-normalized REE diagrams (Fig. 5). They also exhibit depletion of Nb, Ta and Ce, and enrichment of Ba, Th, U and Pb contents in the primitive mantle-normalized spider diagrams (Fig. 5).

The samples of the Wulantaolegai granite show $SiO_2 = 68.6–70.70$ wt %, total $Fe_2O_3 = 1.76–1.90$ wt %, $Na_2O = 5.63–6.30$ wt %, $K_2O = 3.52–3.74$ wt % and CaO = 0.89–1.12 wt % (online Supplementary Material Table S1). In addition, they have low MgO contents of 0.23–0.25 wt % and Mg no. values of 23–24. Theses granites are light peraluminous, with A/CNK from 1.0 to 1.08 (Fig. 4c). In the plot of K_2O versus SiO_2, all samples fall into the high-K calc-alkaline field (Fig. 4b). In the chondrite-normalized REE diagrams, the granite samples show enrichment of LREEs ($(La/Yb)_N = 5.87–6.66$) and negative Eu anomalies (δEu = 0.80–0.82) (Fig. 5). They also exhibit depletion of Ba, Nb, Ce and Sr, and enrichment of Rb, Th, U and Pb contents in the primitive mantle-normalized spider diagrams (Fig. 5).

The samples from the Chahanhada granite show $SiO_2 = 72.76–77.70$ wt %, total $Fe_2O_3 = 0.98–1.26$ wt %, $Na_2O = 4.05–4.77$ wt %, $K_2O = 3.20–3.77$ and CaO = 0.35–0.51 wt % (online Supplementary Material Table S1). In addition, they have low MgO contents of 0.26–0.36 wt % with Mg no. values of 38–40. These granites are peraluminous, with an A/CNK from 1.15 to 1.17 (Fig. 4c). In the plot of K_2O versus SiO_2, all samples fall into the medium to high-K calc-alkaline field (Fig. 4b). Chondrite-normalized REE patterns of these samples show enrichment of LREEs ($(La/Yb)_N = 10.27–12.93$) with obvious Eu anomalies (δEu = 0.49–0.53) (Fig. 5). They exhibit depletion of Ba, Nb, Ce, Sr and Eu, and enrichment of Rb, Th, U, La, Pb and Nd contents in the primitive mantle-normalized spider diagrams as well (Fig. 5).

https://doi.org/10.1017/S0016756822001157 Published online by Cambridge University Press

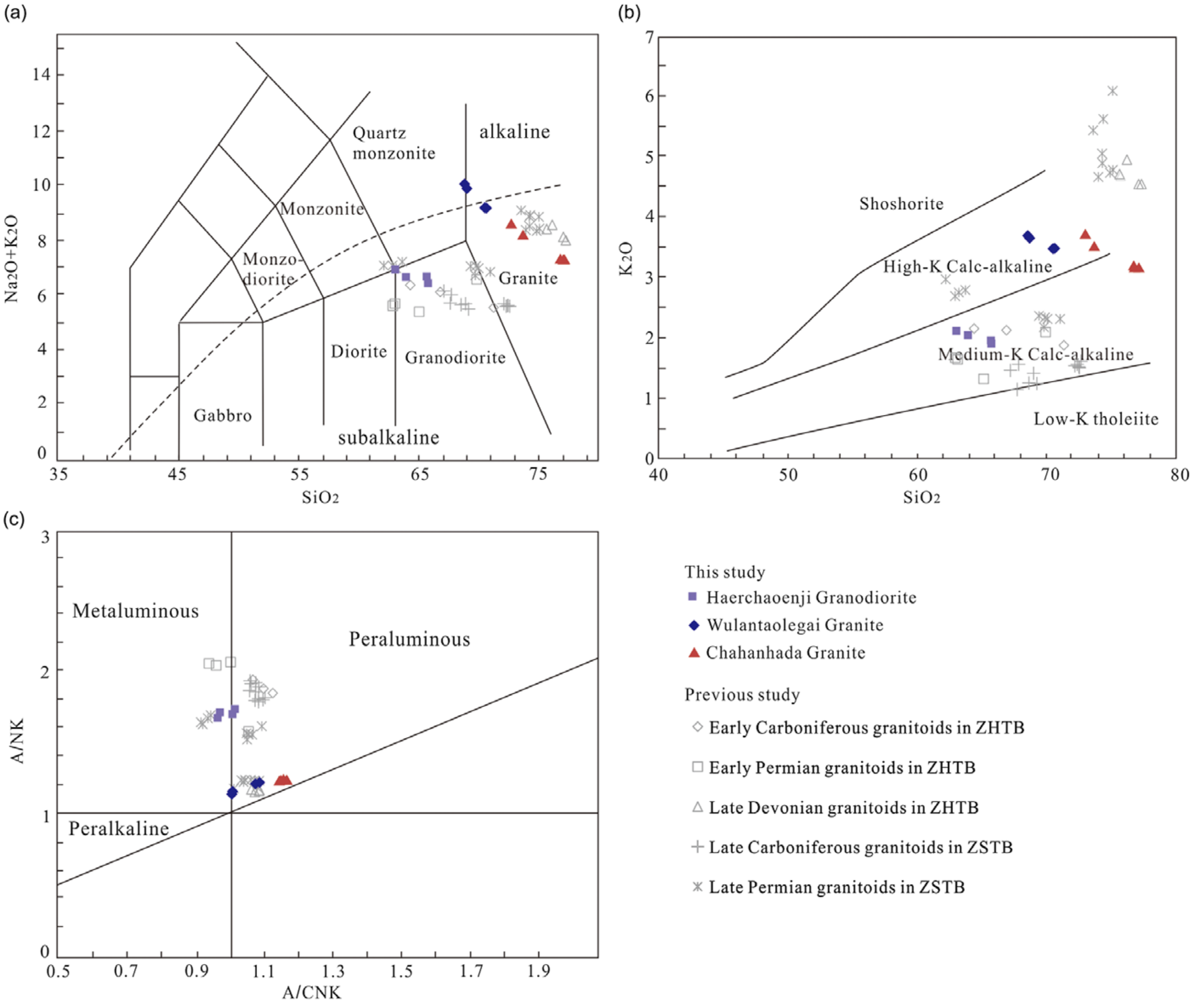

Fig. 4. (Colour online) (a) ($Na_2O + K_2O$) versus SiO_2, (b) K_2O versus SiO_2 and (c) A/NK versus A/CNK plots for investigated samples from the ZSTB. The field boundaries in the three diagrams are from Irvine & Baragar (1971), Peccerillo & Taylor (1976) and Maniar & Piccoli (1989), respectively. Previous data of ZHTB and ZSTB are cited from Shi *et al.* (2014*a*) and Zhang *et al.* (2017).

5.b. U–Pb zircon geochronological data

The results of zircon LA-ICP-MS U–Pb dating are presented in online Supplementary Material Table S3. The zircons separated from the granodiorite (YE-17-69) and granites (YE-17-78, YE-17-88) are mostly colourless, transparent and well crystallized, with grain diameters of 200–300 μm, 150–200 μm and 50–120 μm, respectively (Fig. 6). The length/width ratios of the zircon grains range from 1:1 to 5:1 (YE-17-69), 1:1 to 3:1 (YE-17-78) and 1:1 to 2:1 (YE-17-88), respectively. The CL images revealed that the selected zircons display clear oscillatory zoning and platy structures (Fig. 6). All zircon grains are euhedral to subhedral with prismatic to sub-prismatic shapes (Fig. 6). Moreover, the relatively high Th/U ratios of the three samples (0.43–1.34, 0.37–0.62 and 0.47–1.30, respectively) also suggest a magmatic origin (Hoskin & Schaltegger, 2003). The $^{206}Pb–^{238}U$ weighted average ages of concordant points are 245 ± 5 Ma (MSWD = 0.56, N = 19) for YE-17-69, 237 ± 2 Ma (MSWD = 0.43, N = 25) for YE-17-78 and 245 ± 2 Ma (MSWD = 0.38, N = 17) for YE-17-88.

5.c. Zircon Lu–Hf results

The zircon grains that were previously analysed by U–Pb methods were also analysed for Lu–Hf isotopes on the same spot, and the results are listed in online Supplementary Material Table S2. Fifteen spots on zircons selected from sample YE-17-69 yielded variable $\epsilon_{Hf}(t)$ values between +1.8 and +6.4 (Fig. 7), with Hf model ages (T_{DM}) of 636–837 Ma, and initial $^{176}Hf/^{177}Hf$ ratios from 0.282676 to 0.282807. Fifteen spots on zircons selected from sample YE-17-78 showed variable $\epsilon_{Hf}(t)$ values ranging from +3.3 to +8.7 (Fig. 7), corresponding to T_{DM} ages varying from 545 to 778 Ma, with the initial $^{176}Hf/^{177}Hf$ ratios ranging from 0.282712 to 0.282864. Fifteen spots on zircons from sample YE-17-88 yielded positive $\epsilon_{Hf}(t)$ values ranging from +5.5 to +11.8

https://doi.org/10.1017/S0016756822001157 Published online by Cambridge University Press

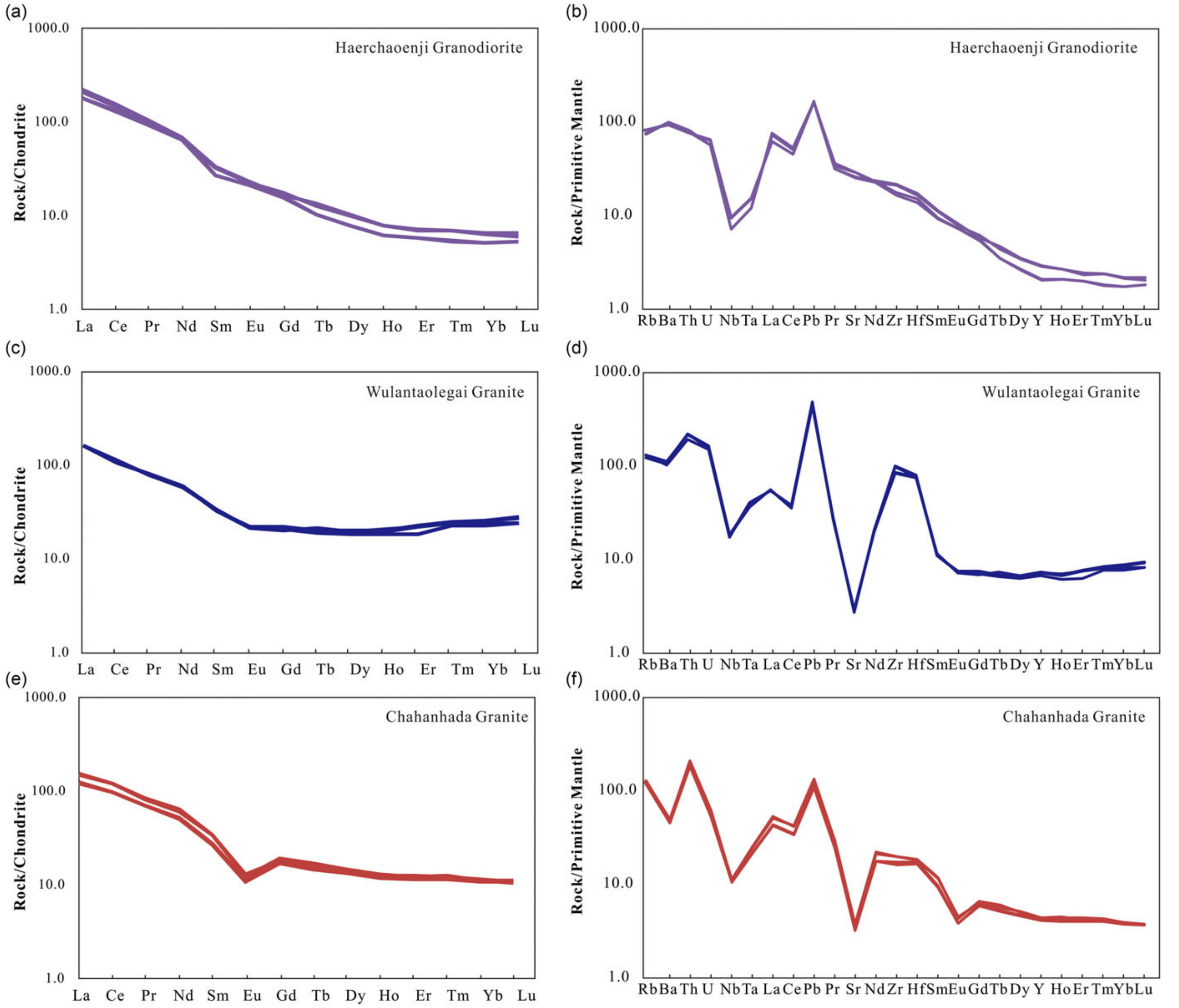

Fig. 5. (Colour online) (a, c, e) Chondrite-normalized REE patterns; the normalization values of chondrite are from Taylor & McLennan (1985). (b, d, f) Primitive mantle-normalized trace-element patterns; data for primitive mantle are from Sun & McDonough (1989).

(Fig. 7), corresponding to young T_{DM} ages from 425 to 729 Ma, and the initial $^{176}Hf/^{177}Hf$ ratios varied between 0.282776 and 0.282955.

6. Discussion

6.a. Geochronological framework of the ZSTB

The geochronological data are important to constrain the magmatic event and further understand the tectonic evolution of the northern Alxa region. In this study, the obtained zircon U–Pb ages are considered to reflect the timing of magmatic events. The zircon U–Pb dating of the samples from three plutons in the ZSTB yielded weighted mean $^{206}Pb–^{238}U$ ages of 237~245 Ma (Fig. 8). These dates provide robust evidence for the presence of early Mesozoic magmatism in the northern Alxa region. Furthermore, we collected previously reported magmatic events in the ZSTB (e.g. Zhang *et al.* 2013; Liu & Zhang, 2014*a*,*b*; Shi *et al.* 2014*a*,*b*; Yang *et al.* 2014; Shi, G. Z. *et al.* 2016; Zheng *et al.* 2016; Xie *et al.* 2021) and revealed several magmatic episodes in the ZSTB (Fig. 9; online Supplementary Material Table S4). Although such late Palaeozoic – early Mesozoic magmatism is successive, the statistical data display three main age peaks at *c.* 270, 250 and 228 Ma (Fig. 9). When these age data are combined, they show multi-stage magmatism in the ZSTB (Fig. 9), implying a long-lived magmatism from late Palaeozoic to early Mesozoic times in response to a prolonged subduction, collision and extension in the central segment of the CAOB.

6.b. Genetic type

Granitoids are commonly classified into I-, A-, S- and M-types based on their source compositions, mineral assemblages and geochemical features (Chappell & White, 2001; Bonin, 2007). The Haerchaoenji granodiorite and Chahanhada granite are similar to typical I-type granitoids. Specifically, these granitoids are

https://doi.org/10.1017/S0016756822001157 Published online by Cambridge University Press

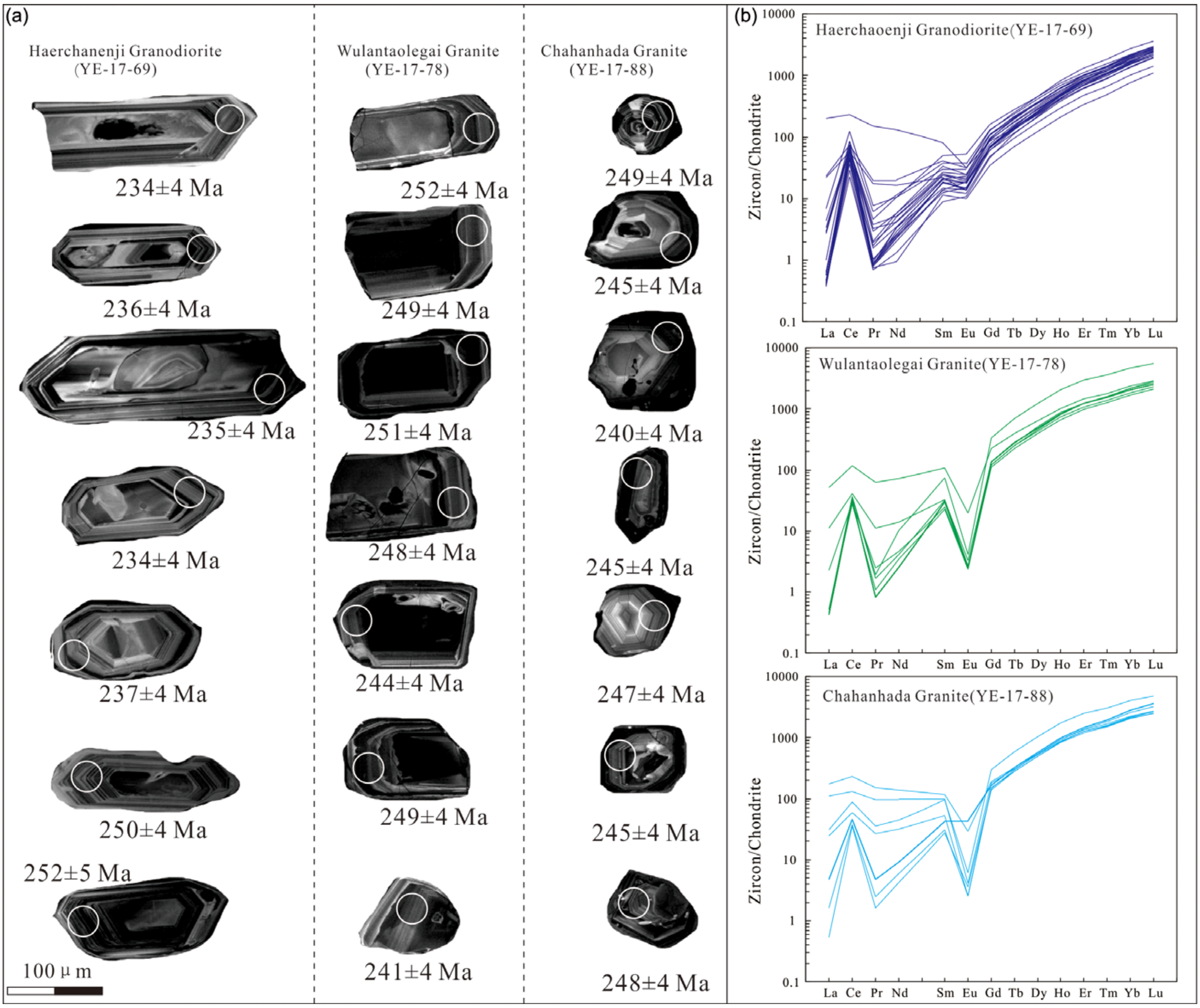

Fig. 6. (Colour online) (a) Cathodoluminescence (CL) images of representative zircons of investigated samples from the ZSTB. (b) Chondrite-normalized REE patterns of the zircons from investigated samples.

metaluminous to weakly peraluminous and medium-K to high-K calc-alkaline with A/CNK and A/NK ratios of 0.97–1.17 and 1.24–1.74, respectively. These features suggest that they represent an I-type or A-type granitoid rather than an S-type (Chappell & White, 1992; Zhang *et al.* 2017; Zhao *et al.* 2020). Moreover, these granitoids have relatively lower 10 000 Ga/Al ratios (1.86–2.34) and Zr + Nb + Ce + Y contents (269.88–347.60 ppm) than A-type granitoids (Whalen *et al.* 1987) (Fig. 10a–d). The negative correlation between P_2O_5 and SiO_2 appears to follow the I-type trend (Fig. 10e). The relatively low Zr and Ce contents of the samples also suggests that these rocks are I-type granitoids. This conclusion can be further supported by the Na_2O versus SiO_2 diagram (Fig. 10f).

However, the Wulantaolegai granite has characteristics more similar to A-type granitoids. These samples have high $K_2O + Na_2O$, FeO^T/MgO, Zr and Ga/Al ratios, which are consistent with those of A-type granitoids (e.g. Dan *et al.* 2014; Ao *et al.* 2019). In addition, the samples have higher 10 000*Ga/Al (2.67–2.74) and Zr + Nb + Ce + Y (1051–1230 ppm), and plot into the A-type granitoid field on the discrimination diagrams (Fig. 10a–d). Thus, the Haerchaoenji granodiorite and Chahanhada granite are considered to be I-type granitoids, while the Wulantaolegai granite is classified as A-type granitoid.

6.c. Temperature–pressure conditions of melting

Zircon saturation thermometry can be used to make an approximate estimate of the temperature of crustal-derived silicic magmas at the early stage of crystallization (Hui *et al.* 2021 and references therein). Zircon saturation temperatures (T_{Zr}) of magma are estimated using zirconium concentrations of melt using the equation from Boehnke *et al.* (2013). Based on the Zr content of the studied samples, the T_{Zr} ranged from 728 to 747 °C (av. 738 °C) in the Haerchaoenji granodiorites, 928 to 981 °C (av. 955 °C) in the Wulantaolegai granites, and 740 to 792 °C (av. 778 °C) in the Chahanhada granites. The mean values of T_{Zr} in the Haerchaoenji granodiorite and Chahanhada granite are consistent with those in typical I-type granites (781 °C, e.g. Chappell & White,

https://doi.org/10.1017/S0016756822001157 Published online by Cambridge University Press

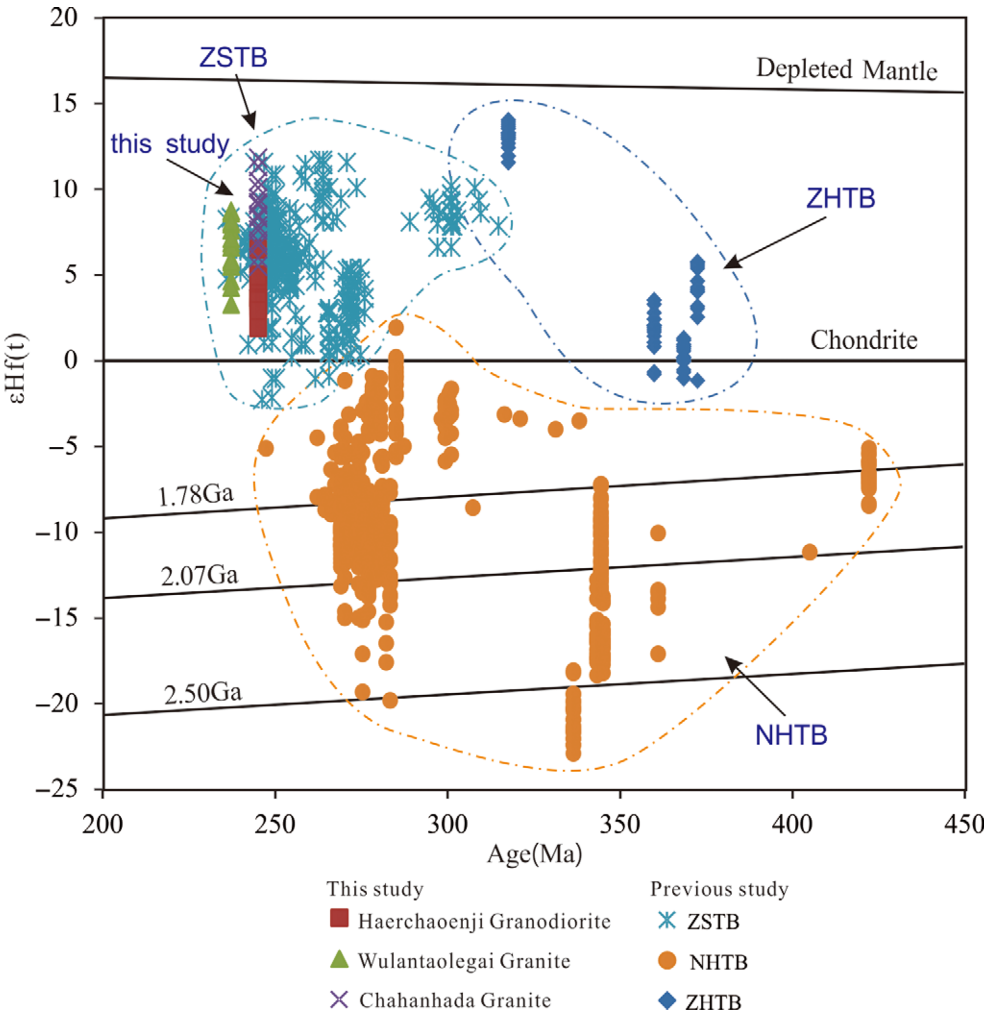

Fig. 7. (Colour online) Zircon Hf isotopic compositions of intrusive rocks from the CAOB. ZSTB – Zongnaishan–Shalazhashan Tectonic Belt; ZHTB – Zhusileng–Hangwula Tectonic Belt; NHTB – Nuoergong–Honggueryulin Tectonic Belt. The $\epsilon_{Hf}(t)$ values are cited from Shi *et al.* (2012, 2014*a*,*b*), Dan *et al.* (2014, 2015, 2016), Ye *et al.* (2016), Zhang, W. *et al.* (2016), Liu *et al.* (2017) and Zhao *et al.* (2020).

1992). The mean value of T_{Zr} in the Wulantaolegai granite points to a hot granitoid (T_{Zr} >800 °C; Miller *et al.* 2003), which is consistent with that of A-type granites (Watson & Harrison, 1983).

With respect to pressure, low Sr contents and Sr/Y ratios, as well as negative Eu anomalies in the Wulantaolegai and Chahanhada granites (online Supplementary Material Table S1), reflect low-pressure conditions of the magma source region (e.g. Martin *et al.* 2005). The coupled observations of the two pressure-dependent ratios, namely Sr/Y and La/Yb, point to a low pressure as well (Fig. 11). The low-pressure conditions inferred for these granites are consistent with their high silica contents as well (e.g. Blundy & Cashman, 2001). In contrast, the Haerchaoenji granodiorites exhibit high Sr and Ba contents with high Sr/Y ratios, low Y and heavy rare earth element (HREE) contents, implying high-pressure conditions (pressure >12 kbar) (e.g. Patiño Douce, 1999; Martin *et al.* 2005; Liu *et al.* 2016).

6.d. Petrogenesis and magma source

6.d.1. The Haerchaoenji and Chahanhada I-type granitoids

The Haerchaoenji granodiorite and Chahanhada granite are calc-alkaline and peraluminous I-type granitoids, which could be formed by: (1) partial melting of pre-existing igneous rocks in the crust (Clemens *et al.* 2011; Topuz *et al.* 2019; Xie *et al.* 2021); (2) mixing of mantle-derived magmas with crustal-derived materials (Clemens *et al.* 2009); and (3) assimilation and fractional crystallization processes of mantle-derived basaltic melts (Barth *et al.* 1995; Quelhas *et al.* 2020).

The investigated samples have Rb/Sr = 0.80–1.00, K/Rb = 326.32–435.50 and Zr/Hf = 35.66–46.95, which differs from the high Rb/Sr (> 5), low K/Rb (110) and low Zr/Hf (20) ratios of fractionated granitoids (Wu *et al.* 2020). The fractional crystallization of mafic melts would leave large amounts of mafic–ultramafic cumulates (Clemens *et al.* 2011), which is obviously different from the field investigation. This supposition is also evidenced by the absence of xenocrystic zircons in the investigated granitoids. In addition, these samples from the Haerchaoenji granodiorite and Chahanhada granite show low MgO (0.26–1.91), Cr (4.25–17.04) and Ni (2.61–6.49) contents and moderate Mg no. values (38–49), similar to those of magma formed by partial melting of thickened lower crust instead of fractional crystallization from the mantle directly (Ao *et al.* 2019; Yomeun *et al.* 2022). Furthermore, the positive correlation of La/Sm versus La and Zr/Nb versus Zr presented by the studied rocks can be produced by either magma mixing or partial melting rather than fractional crystallization (Fig. 11). Commonly, the magma mixing model can generate massive mafic enclaves and geochemical variations (Kemp *et al.* 2007). As mentioned above, there are no mafic microgranular enclaves discovered in the field investigation. The studied samples do not show obvious geochemical variations either. In the

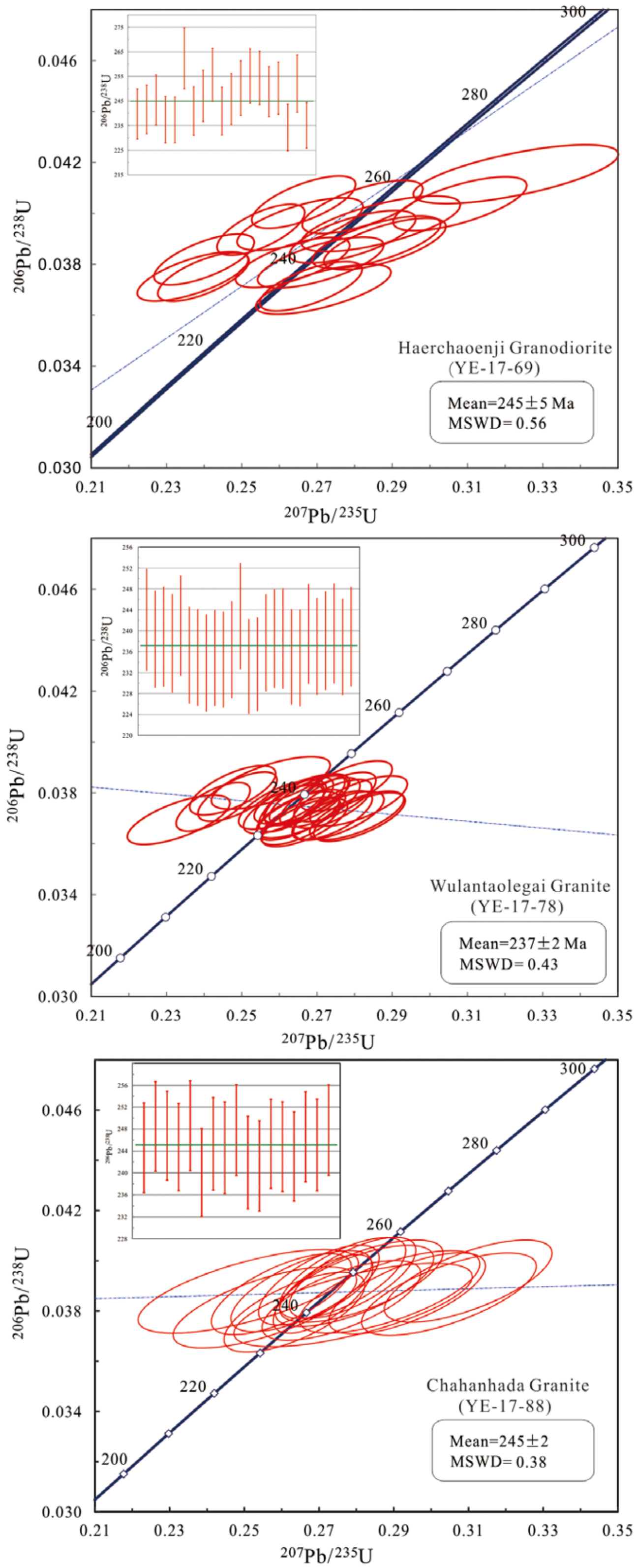

Fig. 8. (Colour online) Zircon U–Pb concordia diagrams and histograms for investigated samples.

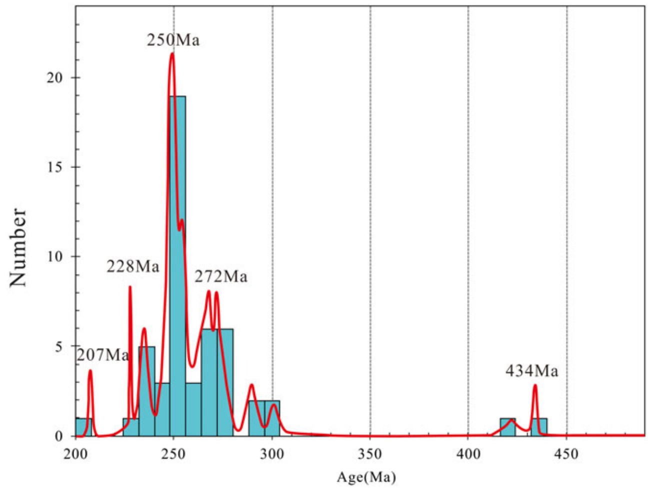

Fig. 9. (Colour online) Histogram of zircon U–Pb ages of the Phanerozoic magmatism in the ZSTB, northern Alxa region. Data sourced from online Supplementary Material Table S4.

Mg no. versus SiO_2 diagram, these samples are also not in conformity with the magma mixing trend (Fig. 12c). The $\epsilon_{Hf}(t)$ values of the Haerchaoenji and Chahanhada granitoids are distinct from the variable $\epsilon_{Hf}(t)$ values of granitoids formed by magma mixing (usually from negative to positive; Griffin *et al.* 2002). The zircon trace elements of the Haerchaoenji and Chahanhada granitoids have medium Th and U contents, indicating a crustal affinity as well. Thus, the Haerchaoenji and Chahanhada granitoids were probably generated by partial melting of pre-existing crustal basements.

Partial melting of different source rocks would generate compositional variations in the magmas that could be visualized in terms of major-element compositions (Altherr *et al.* 2000). The major-element compositions of the Haerchaoenji granodiorites (e.g. high Na_2O and Al_2O_3, medium CaO, low MgO, etc) are similar to those of the intermediate to granitic rocks generated by the partial melting of basaltic (mafic) rocks (Rapp & Watson, 1995; Patiño Douce, 1999). In the major-element feature diagrams (Fig. 12a–e), the granodiorites display a similarity with the experimental melts of amphibolite-bearing mafic rocks (Patiño Douce, 1999; Lu *et al.* 2016, 2017). The low Rb/Ba (0.07–0.08) and Rb/Sr (0.08–0.10) ratios indicate basalt-derived components as well (Fig. 12f). The low Th/La ratios (<0.5) of these granodiorites are also consistent with those of the products yielded by partial melting of mafic crustal sources. The positive zircon $\epsilon_{Hf}(t)$ values between +1.8 and +6.4 (Fig. 7), with young T_{DM} ages of 636–837 Ma, indicate that the granodiorites were mainly derived from Neoproterozoic juvenile mafic crustal materials. In contrast, the Chahanhada granite samples have relatively high Al_2O_3/TiO_2 ratios (52.54–93.76), A/CNK values (1.00–1.17) and low CaO/Na_2O ratios (0.09–0.18), suggesting the derivation from a parental magma that was probably generated by the partial melting of a metasedimentary source (Sylvester, 1998; Zhu, R. Z. *et al.* 2018). In the source discrimination diagrams (Fig. 12), the Chahanhada granites plot into the fields of metagreywacke and metapelite melts. Actually, it is common that the source of I-type granites involves mature sedimentary materials (Zhu, Y. *et al.* 2018). However, the positive zircon $\epsilon_{Hf}(t)$ values ranged from +5.5 to +11.8 (Fig. 7), with young T_{DM} ages of 425–729 Ma, suggesting the significant involvement of juvenile crustal materials. Thus, the Chahanhada granites might have originated from juvenile crust with the input of metasedimentary components.

https://doi.org/10.1017/S0016756822001157 Published online by Cambridge University Press

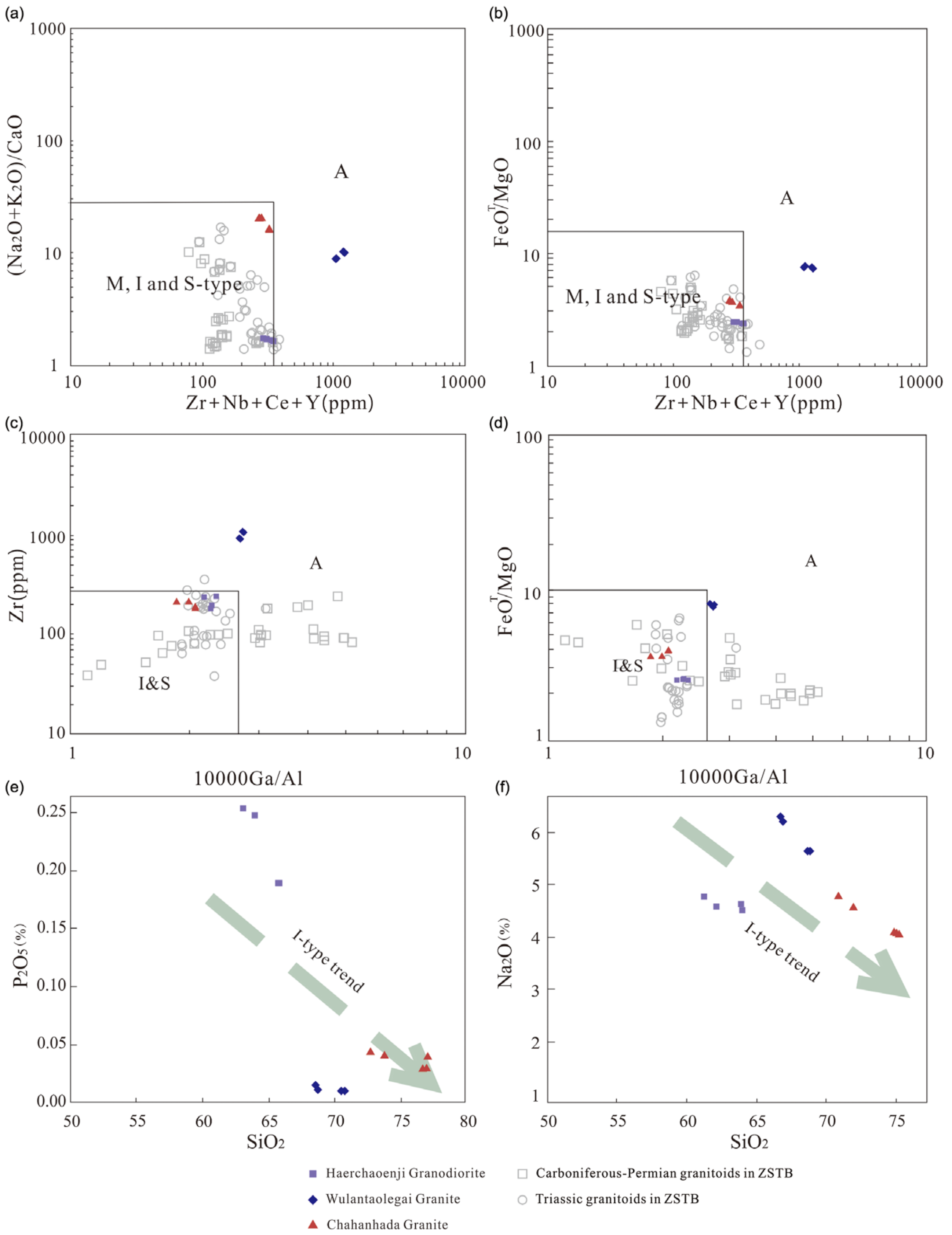

Fig. 10. (Colour online) Petrogenetic discrimination diagrams for early Mesozoic granitoids in the ZSTB. (a) ($K_2O + Na_2O/CaO$) versus Zr + Nb + Ce + Y. (b) FeO^T/MgO versus Zr + Nb + Ce + Y. (c) Zr versus 10 000Ga/Al. (d) FeO^T/MgO versus 10 000Ga/Al. (e) P_2O_5 versus SiO_2. (f) Na_2O versus SiO_2 (a–d are after Whalen *et al*. 1987, and e, f are after Chappell & White, 1992).

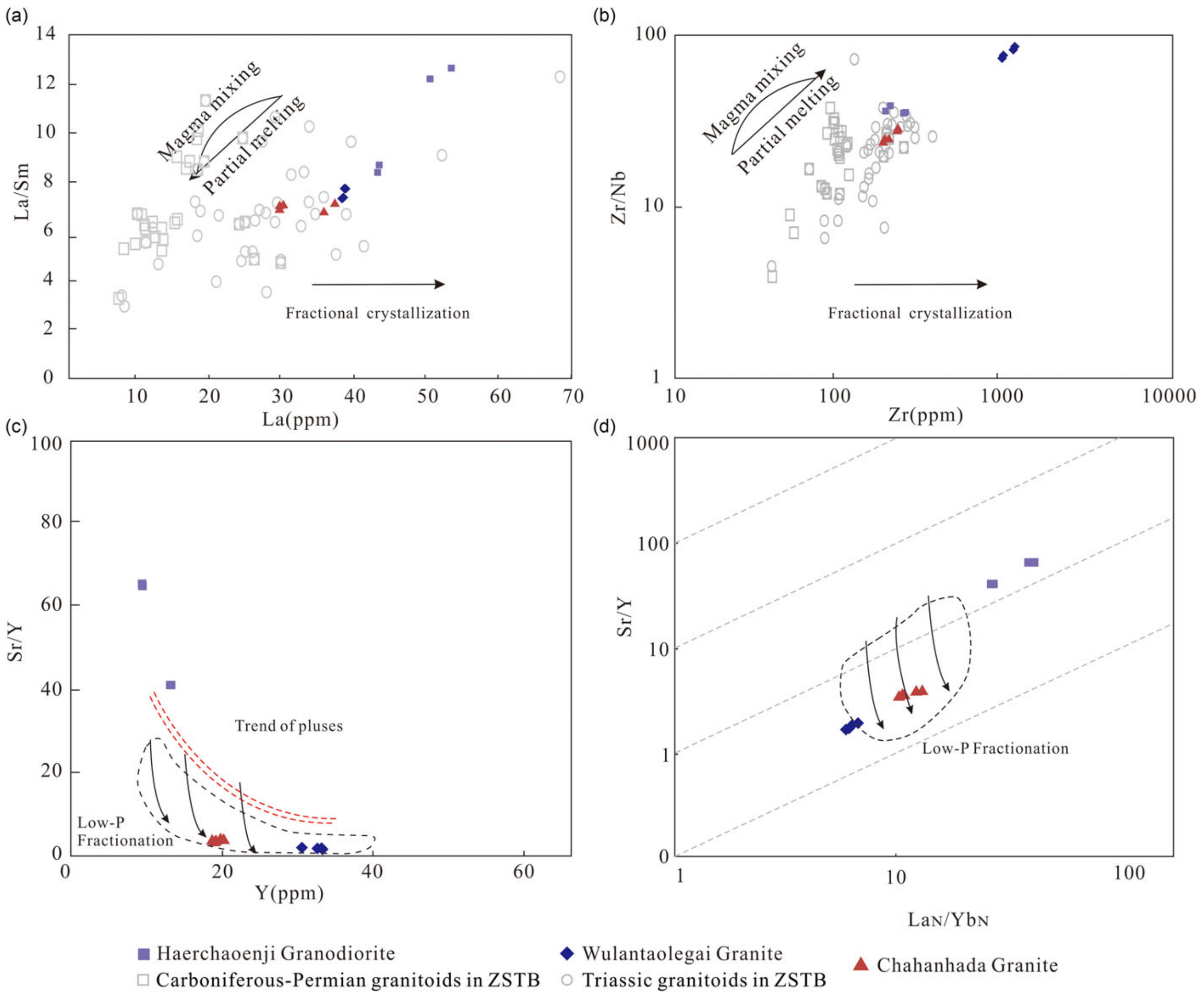

Fig. 11. (Colour online) Plots of (a) La/Sm versus La; (b) Zr/Nb versus Zr; (c) Sr/Y versus Y; and (d) Sr/Y versus La_N/Yb_N (a, b are after Xie *et al.* 2021, and c, d are after Castro *et al.* 2011).

6.d.2. The Wulantaolegai A-type granite

The Wulantaolegai granite displays the features of A-type granite, which is generally attributed to: (1) differentiation of mantle-derived alkaline basalts (Turner *et al.* 1992; Mushkin *et al.* 2003); (2) partial melting of crustal materials at high temperatures (Collins *et al.* 1982; King *et al.* 1997), and (3) a combination of crustal and mantle sources, i.e. crustal assimilation and fractional crystallization of mantle-derived magmas, or magma mixing of mantle-derived melts and crustal magmas (Kemp *et al.* 2005). The Mg no. values and Cr and Ni contents of the Wulantaolegai granites are much lower than those of the mantle-derived melts (Mg no. = 73–81, Cr >1000 ppm, Ni >400 ppm) (Wilson, 1989). The Nb/Ta (8 on average) and Zr/Hf (43 on average) ratios of the Wulantaolegai granites in this study are consistent with those of the crust. The low Nb/Y (0.38–0.41) and Rb/Y (2.37–2.71) ratios also suggest a lower crustal source (Rudnick & Fountain, 1995). Furthermore, the Wulantaolegai granites have higher Y/Nb (2.45–2.60, >1.2), i.e. A2-type granite affinities (Eby, 1992; Frost & Frost, 2011), which also suggests that the magmas were derived from continental crust or underplated basaltic protoliths (Eby, 1992). So far, coeval mantle-derived mafic rocks have not been recognized in the study area. The absence of mafic microgranular enclaves in the Wulantaolegai pluton does not support the model of a combination of crustal and mantle sources. In the Mg no. versus SiO_2 diagram (Fig. 12c), the Wulantaolegai granite samples are not in conformity with the magma mixing trend. In the La/Sm versus La and Zr/Nb versus Zr diagrams, the Wulantaolegai granite samples also display the feature of partial melting processes rather than magma mixing or fractional crystallization (Fig. 11). The Wulantaolegai granite samples have positive $\epsilon_{Hf}(t)$ values ranging from +3.3 to +8.7, indicating a magma source from juvenile crustal basement rather than a mixed source. In addition, the zircon saturation temperatures of the Wulantaolegai granite indicate high-temperature conditions. Thus, the model of partial melting of juvenile crustal materials at high temperatures is reasonable for the petrogenesis of the Wulantaolegai granite.

The relatively low Sr (57.50–62.60 ppm) and high HREE contents, and weakly fractionated HREEs and low Sr/Y ratios (1.72–1.99) suggest these rocks were mainly derived from a crustal source

https://doi.org/10.1017/S0016756822001157 Published online by Cambridge University Press

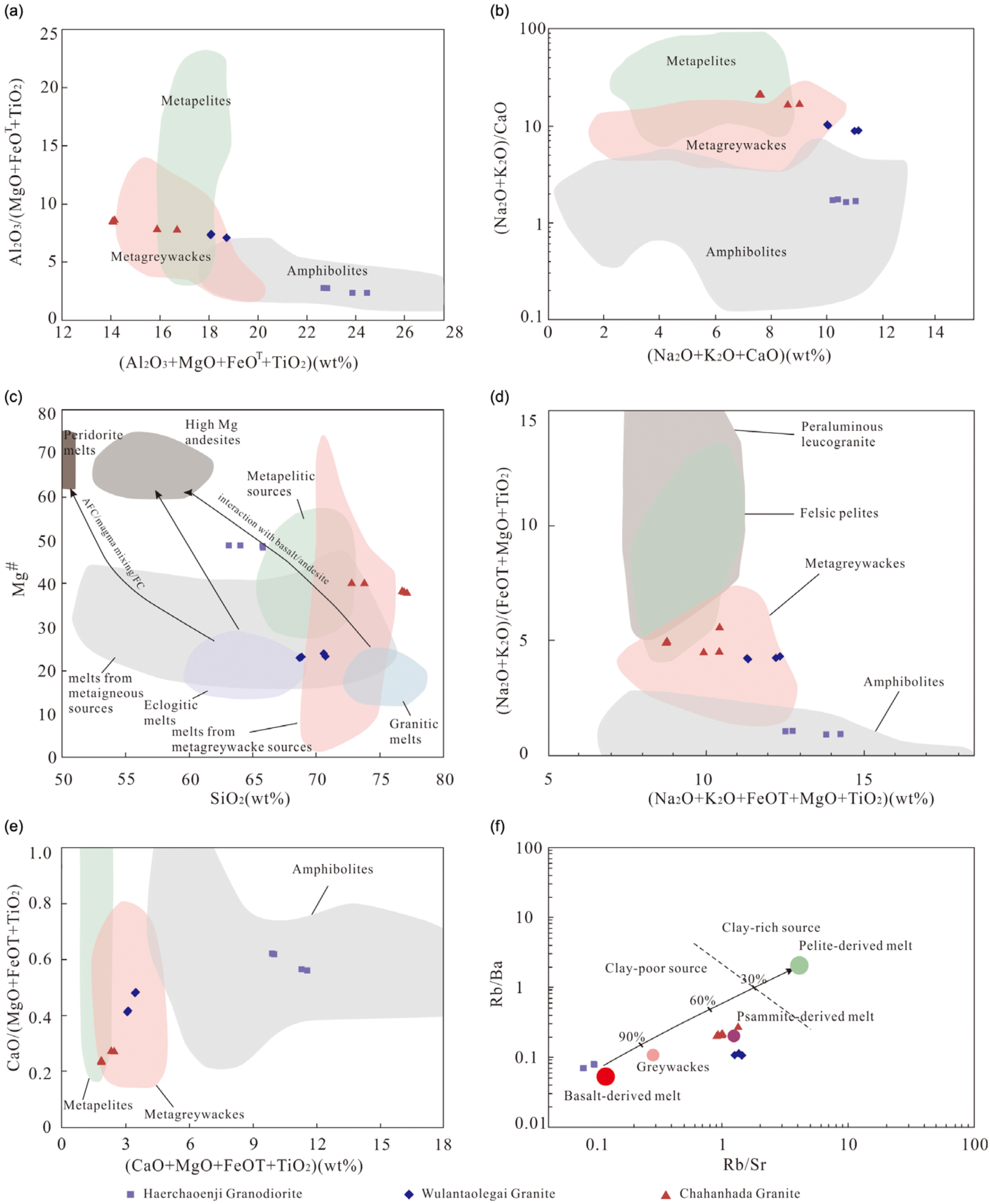

Fig. 12. (Colour online) (a) $Al_2O_3/(MgO + FeO^T + TiO_2)$ versus $Al_2O_3 + MgO + FeO^T + TiO_2$ (Patiño Douce, 1999). (b) $(Na_2O + K_2O)/CaO$ versus $Na_2O + K_2O + CaO$ (Patiño Douce, 1999). (c) Mg no. versus SiO_2 diagram (after Zhu, R. Z. *et al.* 2018; reference fields after Patiño Douce, 1999; Wolf & Wyllie, 1994). (d) $(Na_2O + K_2O)/(FeO^T + MgO + TiO_2)$ versus $(Na_2O + K_2O + FeO^T + MgO + TiO_2)$ (Patiño Douce, 1999). (e) $CaO/(MgO + FeO^T + TiO_2)$ versus $(CaO + MgO + FeO^T + TiO_2)$ (Patiño Douce, 1999). (f) Rb/Ba versus Rb/Sr (Patiño Douce, 1999).

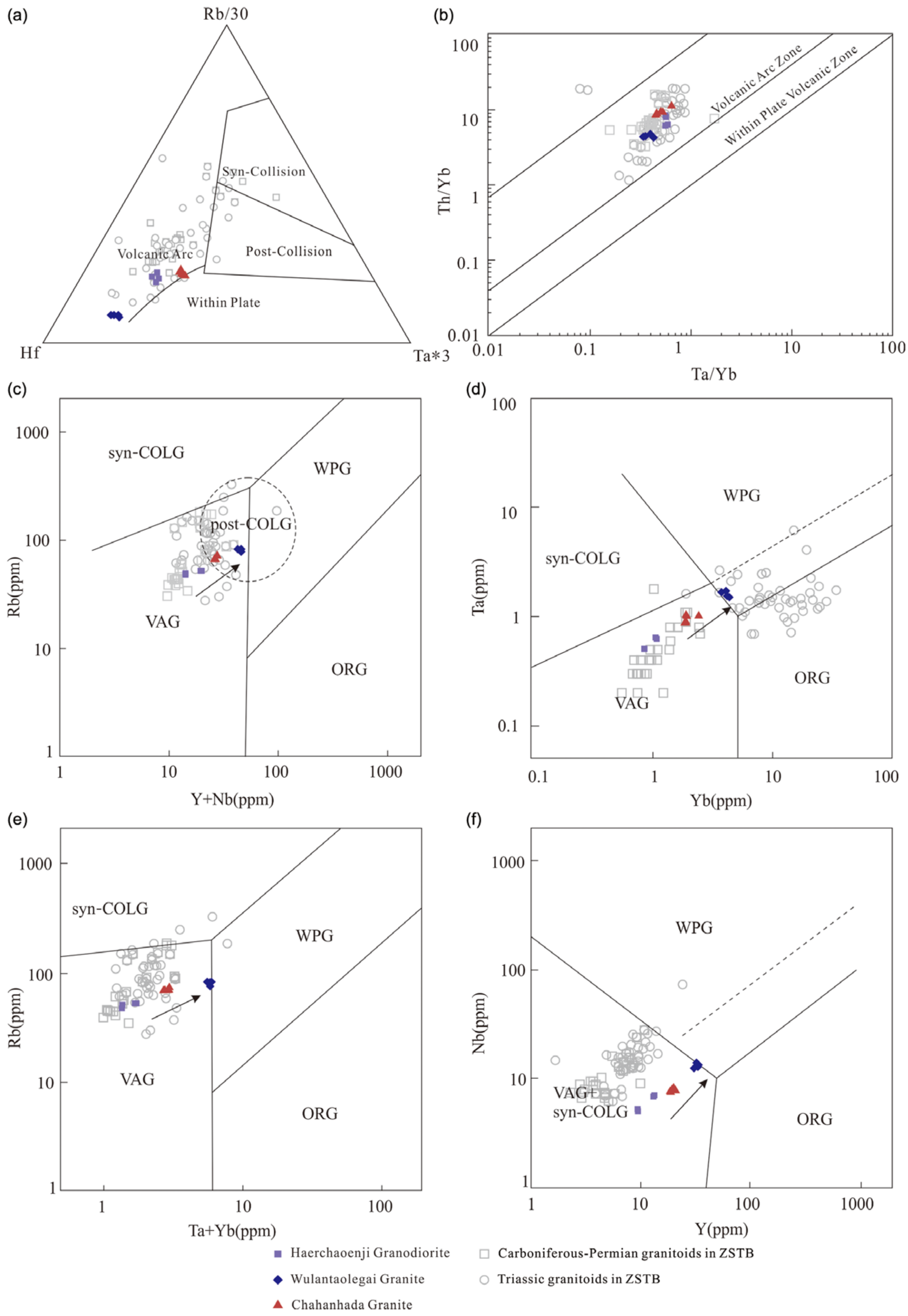

Fig. 13. (Colour online) Tectonic setting discrimination diagrams for the early Mesozoic granitoids in the ZSTB. (a) Ta*3–Rb/30–Hf ternary plot (Harris *et al.* 1987). (b) Th/Yb versus Ta/Yb (Gorton & Schandl, 2000). (c) Rb versus Y + Nb (Pearce *et al.* 1984; Pearce, 1996). (d) Ta versus Yb (Pearce *et al.* 1984). (e) Rb versus Ta + Yb (Pearce *et al.* 1984). (f) Nb versus Y (Pearce *et al.* 1984). Syn-COLG – syn-collision granites; VAG – volcanic arc granites; WPG – within plate granites; ORG – ocean ridge granites.

https://doi.org/10.1017/S0016756822001157 Published online by Cambridge University Press

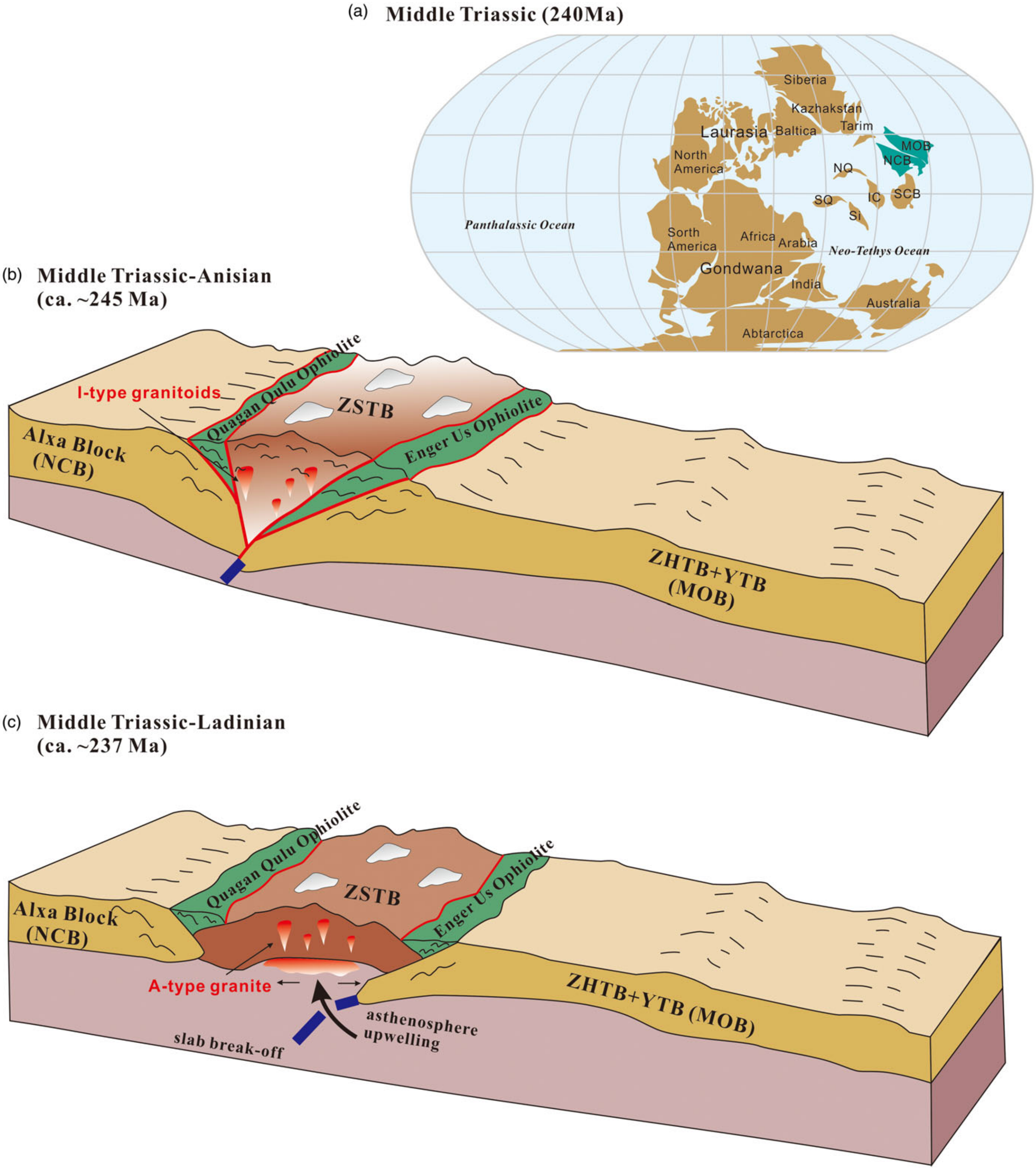

Fig. 14. (Colour online) (a) Palaeogeographic reconstructions of Eastern Asian blocks (modified after Huang *et al.* 2018). (b, c) Diagrams illustrate the tentative tectonic scenario showing the Middle Triassic evolution of the ZSTB and adjacent areas. IC – Indochina Block; MOB – Mongolian Block; NCB – North China Block; NQ – North Qiangtang block; SCB – South China Block; Si – Sibumasu block; SQ – South Qiangtang block.

above the garnet stability depth (Cai *et al.* 2011*b*), and the high Rb/Y ratios (2.37–2.71) and low Nb/Y ratios (0.38–0.41) display the approach to the upper crustal source (Taylor & McLennan, 1985). These features suggest that the source region of these granites is relatively shallow. In the source discrimination diagrams (Fig. 12), the Wulantaolegai granites variably fall into the overlapping fields of the partial melts of metagreywackes, psammite and meta-igneous rocks. The positive zircon $\epsilon_{Hf}(t)$ values between +3.3 and +8.7 (Fig. 7) with young T_{DM} ages of 545–778 Ma suggest the involvement of juvenile mafic crust for the Wulantaolegai granites,

https://doi.org/10.1017/S0016756822001157 Published online by Cambridge University Press

which is similar to other granitoids in the southern CAOB (e.g. Shi *et al.* 2014*a*; Xie *et al.* 2021). The low Th/La ratios (<0.5) of the A-type granites in this study are also consistent with that of the partial melting products of mafic crustal sources. The variable zircon $\epsilon_{Hf}(t)$ units of these granites were probably caused by some recycled sediments in the magma source.

6.e. Tectonic setting and geological implications

6.e.1. Tectonic setting

In this study, the investigated granitoids display the common features of volcanic arc granites, such as the depletion of Nb, Ta and enrichment of large ion lithophile elements with low Sr/Y and $(La/Yb)_N$ (e.g. Zhao, Y. *et al.* 2017; Xie *et al.* 2021). On the Th/Yb versus Ta/Yb and Ta*3–Rb/30–Hf ternary diagram, these granitoids also display the affinity of volcanic arc granitoids, analogous to a subduction-related compressional setting (Fig. 13a, b). On the tectonic discrimination diagrams, the Haerchaoenji and Chahanhada granitoid samples plot in the volcanic arc field, while the Wulantaolegai samples show trends from the arc to post-collisional fields (Fig. 13a–f). These findings suggest that these granitoids either formed in a subduction-related setting, or a post-collisional setting with arc-like geochemical signatures which are inherited from a previous arc source. In this study, we prefer a post-collisional setting with arc affinity based on the following regional data: (1) the magmatism ranging from late Carboniferous to middle–late Permian times exhibits a marked petrogenetic, geochemical and isotopic transition and trends from the subduction to post-collisional fields (e.g. Zhang *et al.* 2013; Shi *et al.* 2014*a*,*b*; Xu, D. Z. *et al.* 2014; Yang *et al.* 2014; Zheng *et al.* 2014; Chen *et al.* 2015; Xie *et al.* 2015; Liu *et al.* 2017, 2018); (2) the regional unconformity and the change of sedimentary facies also suggest that a significant tectonic event happened during early–middle Permian time (Zhang, 2019); (3) the palaeomagnetic, provenance and palaeontological studies further suggest that the PAO in the northern Alxa region closed before earliest Mesozoic time (Fig. 14a) (Pu *et al.* 2013; Huang *et al.* 2018; Zhang *et al.* 2018).

Therefore, the Middle Triassic granitoids in the ZSTB are interpreted as post-collisional granites (Fig. 14b, c). Furthermore, in the scenario of subduction and subsequent continental collision processes, asthenospheric mantle upwelling would be inevitable owing to slab roll-back or break-off (Ersoy *et al.* 2017; Collins *et al.* 2020). The Wulantaolegai A-type granite was probably generated by an extensional setting in response to slab break-off during the final amalgamation (Fig. 14c).

6.e.2. Geological implications

As mentioned above, extensive studies have been carried out on the closure of the PAO, producing a large quantity of data and competing models (e.g. Xiao *et al.* 2013, 2015, 2018; Eizenhöfer *et al.* 2014, 2015*a*,*b*; Li *et al.* 2015, 2016*a*, 2017; Liu *et al.* 2017, 2018, 2019*a*,*b*; Han & Zhao, 2018; Eizenhöfer & Zhao, 2018; Du *et al.* 2019; Shen *et al.* 2019; Zheng *et al.* 2019; Niu *et al.* 2021). Generally, the western segment of the PAO closed along the Tianshan Orogen during the Carboniferous–early Permian period (e.g. Han & Zhao, 2018; Zheng *et al.* 2019). However, the eastern segment of the PAO closed during late Permian to Middle Triassic times along the Solonker Suture Belt (e.g. Eizenhöfer *et al.* 2014, 2015*a*,*b*; Li *et al.* 2015, 2016*a*, 2017; Eizenhöfer & Zhao, 2018). Recent studies demonstrated that the central segment of the PAO closed at *c.* 280–265 Ma (Liu *et al.* 2016, 2017, 2018; Zhao *et al.* 2018), which is also consistent with this study. Combining these data together, we still tend to support the scissor-like closure manner, which is in accordance with previous studies (e.g. Boucot *et al.* 2013; Xiao *et al.* 2015; Zhao *et al.* 2018; Han & Zhao, 2018; Shen *et al.* 2019). This conclusion is also supported by the constraints from sedimentary strata (Zhao, Y. L. *et al.* 2016; Liu *et al.* 2019*a*; Du *et al.* 2019), syn-collisional magmatic rocks (Wang *et al.* 2015; Chen *et al.* 2017; Ma *et al.* 2017), structural evidence (Xiao *et al.* 2015) and plate reconstruction (Domeier & Torsvik, 2014; Domeier, 2018).

In order to decipher the nature of the different tectonic units of the northern Alxa region, we collected comprehensive Hf isotopic data in this region (Fig. 7) (Shi *et al.* 2012, 2014*a*,*b*; Dan *et al.* 2014, 2015, 2016; Ye *et al.* 2016; Zhang, W. *et al.* 2016; Liu *et al.* 2017; Zhao *et al.* 2020). It turns out that the magmatic rocks from the ZHTB and ZSTB have the most positive to low negative $\epsilon_{Hf}(t)$ values and relatively young Hf model ages (Fig. 7), suggesting a juvenile nature for the basement (Shi *et al.* 2014*a*,*b*; Zhao *et al.* 2020). Significantly, these characteristics are similar to those of the granitoids in the CAOB (Guo *et al.* 2007; Cao *et al.* 2011, 2012; Meng *et al.* 2011; Li *et al.* 2012, 2013). However, the magmatic rocks from the southernmost NHTB display negative $\epsilon_{Hf}(t)$ values and ancient Hf model ages (Fig. 7), indicating an ancient nature for the basement (Zhang, J. J. *et al.* 2015; Ye *et al.* 2016). Therefore, the juvenile nature of the ZHTB and ZSTB is similar to the CAOB (Shi *et al.* 2014*a*,*b*; Zhang, J. J. *et al.* 2015; Xie *et al.* 2021), but is different from the Alxa Block (NHTB). This conclusion is further reinforced by whole-rock Nd isotopic studies of the Phanerozoic granitoids and volcanic rocks (e.g. Dolgopolova *et al.* 2013; Shi *et al.* 2014*a*), and obvious differences in magmatism record and Precambrian rock constitution (e.g. Geng & Zhou, 2010, 2011; Shi *et al.* 2014*a*). Thus, the boundary of the CAOB and Alxa Block is most likely the border between the ZSTB and NHTB (Badain Jaran fault or Qagan Qulu Ophiolite Belt) rather than the Enger Us belt previously proposed (e.g. Shi, 2015; Zhang, J. J. *et al.* 2015). On a larger scale, this boundary is most likely the central segment of the Tianshan–Solonker suture zone, which connects the northern CAOB with the southern Tarim and North China cratons.

7. Conclusion

(1) New LA-ICP-MS zircon U–Pb dating results have revealed the Middle Triassic magmatism in the Zongnaishan and Shalazhashan areas: the Haerchaoenji granodiorite (245 ± 5 Ma), the Wulantaolegai granite (237 ± 2 Ma) and the Chahanhada granite (245 ± 2 Ma). This study and previous data provide evidence of a prolonged mafic–intermediate magmatism in the ZSTB related to the subduction and closure of the PAO.

(2) The Haerchaoenji granodiorite and Chahanhada granite are classified as I-type granitoids, while the Wulantaolegai granite is considered to be an A-type granite. They were probably derived from partial melting of juvenile crustal materials, inferred from the variable positive Hf isotopic signature and young T_{DM} model ages. The major-element compositions of the Chahanhada granite and Wulantaolegai granites suggest input of a metasedimentary component as well.

(3) Based on the compilation of magmatic, sedimentary, palaeomagnetic and palaeobiogeographic evidence, we propose that the Middle Triassic granitoids in this study were formed in a post-collisional setting, and the arc affinity was probably inherited from recycled subduction-related materials.

https://doi.org/10.1017/S0016756822001157 Published online by Cambridge University Press

(4) The findings of this study support the scissor-like closure mode of the PAO as well as the different tectonic affinities of the ZHTB + ZSTB and NHTB.

Supplementary material. To view supplementary material for this article, please visit https://doi.org/10.1017/S0016756822001157

Acknowledgements. This work was supported by the National Natural Science Foundation of China [grant number 41802119, 41330315, 41972153 and 42072132], Special Projects of China Geological Survey [grant number 121201011000161111], Natural Science Foundation of Shaanxi [grant number 2019JQ-088 and 2021JQ-591], China Postdoctoral Science Foundation [grant number 2019M663779] and Special Scientific Research Programme of Shaanxi Provincial Department of Education [grant number18JK0518].

Conflict of interest. None.

References

Albarède F, Scherer EE, Blichert TJ, Rosing M, Simionovici A and Bizzarro M (2006) γ–ray irradiation in the early Solar System and the conundrum of the ^{176}Lu decay constant. *Geochimica et Cosmochimica Acta* **70**, 1261–70.

Altherr R, Holl A, Hegner E, Langer C and Kreuzer H (2000) High-potassium, calc-alkaline I-type plutonism in the European Variscides: northern Vosges (France) and northern Schwarzwald (Germany). *Lithos* **50**, 51–73.

Ao WH, Zhao Y, Zhang YK, Zhai MG, Zhang H, Zhang RY, Wang Q and Sun Y (2019) The Neoproterozoic magmatism in the northern margin of the Yangtze Block: insights from Neoproterozoic (950–706 Ma) gabbroic-granitoid rocks of the Hannan Complex. *Precambrian Research* **333**, 105442. doi: 10.1016/j.precamres.2019.105442.

Barth AP, Wooden JL, Tosdal RM and Morrison J (1995) Crustal contamination in the petrogenesis of a calc-alkalic rock series: Josephine Mountain intrusion, California. *Geological Society of America Bulletin* **107**, 201–12.

Bea F, Montero P, Molina JF, Scarrow JH, Cambeses A and Moreno JA (2018) Lu-Hf ratios of crustal rocks and their bearing on zircon Hf isotope model ages: the effects of accessories. *Chemical Geology* **484**, 179–90.

BGMRIM (Bureau of Geology and Mineral Resources of Inner Mongolia Autonomous Region) (1991) *Regional Geology of Inner Mongol Autonomous Region*. Beijing: Geological Publishing House (in Chinese).

Blichert-Toft J and Albarède F (1997) The Lu–Hf geochemistry of chondrites and the evolution of the mantle–crust system. *Earth and Planetary Science Letters* **148**, 243–58.

Blundy J and Cashman K (2001) Ascent-driven crystallization of dacite magmas at Mount St Helens, 1980–1986. *Contributions to Mineralogy and Petrology* **140**, 631–50.

Boehnke P, Watson EB, Trail D, Harrison TM and Schmitt AK (2013) Zircon saturation re-revisited. *Chemical Geology* **351**, 324–34.

Bonin B (2007) A-type granites and related rocks: evolution of a concept, problems and prospects. *Lithos* **97**, 1–29.

Boucot AJ, Chen X and Scotese CR (2013) *Phanerozoic Paleoclimate: An Atlas of Lithologic Indicators of Climate*. SEPM, Concepts in Sedimentology and Paleontology, vol. 11, 478 pp.

Bu JJ, Niu ZJ, Wu J and Duan XF (2012) Sedimentary characteristics and age of Amushan Formation in Ejin Banner and its adjacent areas, western Inner Mongolia. *Geological Bulletin of China* **31**, 1669–83 (in Chinese with English abstract).

Cai KD, Sun M, Yuan C, Long XP and Xiao WJ (2011a) Geological framework and Paleozoic tectonic history of the Chinese Altai, NW China: a review. *Russian Geology and Geophysics* **52**, 1585–99.

Cai KD, Sun M, Yuan C, Zhao GC, Xiao WJ, Long XP and Wu FY (2011b) Prolonged magmatism, juvenile nature and tectonic evolution of the Chinese Altai, NW China: evidence from zircon U–Pb and Hf isotopic study of Paleozoic granitoids. *Journal of Asian Earth Sciences* **42**, 949–68.

Cao HH, Xu WL, Pei FP, Guo PY and Wang F (2012) Permian tectonic evolution of the eastern section of the northern margin of the North China Plate: constraints from zircon U–Pb geochronology and geochemistry of the volcanic rocks. *Acta Petrologica Sinica* **28**, 2733–50 (in Chinese with English abstract).

Cao HH, Xu WL, Pei FP and Zhang XZ (2011) Permian tectonic evolution in Southwestern Khanka massif: evidence from zircon U–Pb chronology, Hf isotope and geochemistry of gabbro and diorite. *Acta Geologica Sinica (English Edition)* **85**, 1390–402.

Castro A, Moreno-Ventas I, Fernández C, Vujovich G, Gallastegui G, Heredia N, Martino RD, Becchio R, Corretgé LG, Díaz-Alvarado J, Such P, García-Arias M and Liu DY (2011) Petrology and SHRIMP U-Pb zircon geochronology of Cordilleran granitoids of the Bariloche area, Argentina. *Journal of South American Earth Sciences* **32**, 508–30.

Chappell BW and White AJR (1992) I- and S-type granites in the Lachlan Fold Belt. *Transactions of the Royal Society of Edinburgh: Earth Sciences* **83**, 1–26.

Chappell BW and White AJR (2001) Two contrasting granite types: 25 years later. *Australian Journal of Earth Sciences* **48**, 489–99.

Charvet J, Shu LS, Laurent-Charvet S, Wang B, Faure M, Cluzel D, Chen Y and De Jong K (2011) Palaeozoic tectonic evolution of the Tianshan belt, NW China. *Science China: Earth Sciences* **54**, 166–84.

Chen B, Jahn BM and Tian W (2009) Evolution of the Solonker suture zone: constraints from zircon U-Pb ages, Hf isotopic ratios and whole-rock Nd-Sr isotope compositions of subduction- and collision-related magmas and forearc sediments. *Journal of Asian Earth Sciences* **34**, 245–57.

Chen C, Ren YS, Zhao HL, Yang Q and Shang QQ (2017) Age, tectonic setting, and metallogenic implication of Phanerozoic granitic magmatism at the eastern margin of the Xing'an-Mongolian Orogenic Belt, NE China. *Journal of Asian Earth Sciences* **144**, 368–83.

Chen GC, Shi JZ, Jiang T, Zhang HY, Li W and Wang BW (2015) LA-ICP-MS zircon U-Pb dating and geochemistry of granitoids in Tamusu, Alxa Right Banner, Inner Mongolia. *Geological Bulletin of China* **34**, 1884–96 (in Chinese with English abstract).

Chen Y, Wu TR, Gan LS, Zhang ZC and Fu B (2019) Provenance of the early to mid-Paleozoic sediments in the northern Alxa area: implications for tectonic evolution of the southwestern Central Asian Orogenic Belt. *Gondwana Research* **67**, 115–30.

Clemens JD, Darbyshire DPF and Flinders J (2009) Sources of post-orogenic calcalkaline magmas: the Arrochar and Garabal Hill–Glen Fyne complexes, Scotland. *Lithos* **112**, 524–42.

Clemens JD, Stevens G and Farina F (2011) The enigmatic sources of I-type granites: the peritectic connexion. *Lithos* **126**, 174–81.

Collins WJ, Beams SD, White AJR and Chappell BW (1982) Nature and origin of A-type granites with particular reference to southeastern Australia. *Contributions to Mineralogy and Petrology* **80**, 189–200.

Collins WJ, Huang HQ, Bowden P and Kemp AIS (2020) Repeated S–I–A-type granite trilogy in the Lachlan Orogen, and geochemical contrasts with A-type granites in Nigeria: implications for petrogenesis and tectonic discrimination. In *Post-Archean Granitic Rocks: Petrogenetic Processes and Tectonic Environments* (eds V Janoušek, B Bonin, WJ Collins, F Farina and P Bowden), pp. 53–76. Geological Society of London, Special Publication no. 491.

Cope T, Ritts BD, Darby BJ, Fildani A and Graham SA (2005) Late Paleozoic sedimentation on the northern margin of the North China block: implications for regional tectonics and climate change. *International Geology Review* **47**, 270–96.

Dan W, Li XH, Wang Q, Tang GJ and Liu Y (2014) An Early Permian (ca. 280 Ma) silicic igneous province in the Alxa Block, NW China: a magmatic flare-up triggered by a mantle-plume. *Lithos* **204**, 144–58.

Dan W, Li XH, Wang Q, Wang XC, Wyman DA and Liu Y (2016) Phanerozoic amalgamation of the Alxa Block and North China Craton: evidence from Paleozoic granitoids, U–Pb geochronology and Sr–Nd–Pb–Hf–O isotope geochemistry. *Gondwana Research* **32**, 105–21.

Dan W, Wang Q, Wang XC, Liu Y, Wyman DA and Liu YS (2015) Overlapping Sr–Nd–Hf–O isotopic compositions in Permian mafic enclaves and host granitoids in Alxa Block, NW China: evidence for crust–mantle interaction and implications for the generation of silicic igneous provinces. *Lithos* **230**, 133–45.

Dolgopolova A, Seltmann R, Armstrong R, Belousova E, Pankhurst RJ and Kavalieris I (2013) Sr-Nd-Pb-Hf isotope systematics of the Hugo Dummett Cu-Au porphyry deposit (Oyu Tolgoi, Mongolia). *Lithos* **164**, 47–64.

https://doi.org/10.1017/S0016756822001157 Published online by Cambridge University Press

Domeier M (2018) Early Paleozoic tectonics of Asia: towards a full-plate model. *Geoscience Frontiers* **9**, 789–862.

Domeier M and Torsvik TH (2014) Plate tectonics in the late Paleozoic. *Geoscience Frontiers* **5**, 303–50.

Du QX, Han ZZ, Shen X, Han C, Song ZG, Gao LH, Han M and Zhong WJ (2019) Geochronology and geochemistry of Permo-Triassic sandstones in eastern Jilin Province (NE China): implications for final closure of the Paleo-Asian Ocean. *Geoscience Frontiers* **10**, 683–704.

Eby GN (1992) Chemical subdivision of the A-type granitoids: petrogenetic and tectonic implications. *Geology* **20**, 641–4.

Eizenhöfer PR and Zhao GC (2018) Solonker Suture in East Asia and its bearing on the final closure of the eastern segment of the Palaeo-Asian Ocean. *Earth-Science Reviews* **186**, 153–72.

Eizenhöfer PR, Zhao GC, Sun M, Zhang J, Han YG and Hou WZ (2015a) Geochronological and Hf isotopic variability of detrital zircons in Paleozoic strata across the accretionary collision zone between the North China craton and Mongolian arcs and tectonic implications. *Geological Society of America Bulletin* **127**, 1422–36.

Eizenhöfer PR, Zhao GC, Zhang J, Han YG, Hou WZ, Liu DX and Wang B (2015b) Geochemical characteristics of the Permian basins and their provenances across the Solonker Suture Zone: assessment of net crustal growth during the closure of the Palaeo-Asian Ocean. *Lithos* **224–225**, 240–55.

Eizenhöfer PR, Zhao G, Zhang J and Sun M (2014) Final closure of the Paleo-Asian Ocean along the Solonker Suture Zone: constraints from geochronological and geochemical data of Permian volcanic and sedimentary rocks. *Tectonics* **33**, 441–63.

Ersoy EY, Palmer MR, Genç ŞC, Prelević D, Akal C and Uysal İ (2017) Chemo-probe into the mantle origin of the NW Anatolia Eocene to Miocene volcanic rocks: implications for the role of, crustal accretion, subduction, slab roll-back and slab break-off processes in genesis of post-collisional magmatism. *Lithos* **288–289**, 55–71.

Frost CD and Frost BR (2011) On ferroan (A-type) granitoids: their compositional variability and modes of origin. *Journal of Petrology* **52**, 39–53.

Geng YS and Zhou XW (2010) Early Neoproterozoic granite events in Alxa area of Inner Mongolia and their geological significance: evidence from geochronology. *Acta Mineralogica et Petrologica* **29**, 779–95 (in Chinese with English abstract).

Geng YS and Zhou XW (2011) Characteristics of geochemistry and zircon Hf isotope of the Early Neoproterozoic granite in Alax area, Inner Mongolia. *Acta Petrologica Sinica* **27**, 897–908.

Gorton MP and Schandl ES (2000) From continents to island arcs: a geochemical index of tectonic setting for arc-related and within-plate felsic to intermediate volcanic rocks. *Canadian Mineralogist* **38**, 1065–73.

Griffin WL, Wang X, Jackson SE, Pearson NJ, O'Reilly SY, Xu X and Zhou X (2002) Zircon chemistry and magma mixing, SE China: in-situ analysis of Hf isotopes, Tonglu and Pingtan igneous complexes. *Lithos* **61**, 237–69.

Guo F, Nakamuru E, Fan WM, Kobayoshi K and Li CW (2007) Generation of Palaeocene adakitic andesites by magma mixing; Yanji area, NE China. *Journal of Petrology* **48**, 661–92.

Han YG and Zhao GC (2018) Final amalgamation of the Tianshan and Junggar orogenic collage in the southwestern Central Asian Orogenic Belt: constraints on the closure of the Paleo-Asian Ocean. *Earth-Science Reviews* **186**, 129–52.

Harris RA, Stone DB and Turner DL (1987) Tectonic implications of paleomagnetic and geochronologic data from the Yukon-Koyukuk province, Alaska. *Geological Society of America Bulletin* **99**, 362–75.

He DF, Dong Y, Xu X, Chen JL, Liu XM and Li W (2018) Geochemistry, geochronology and Hf isotope of granitoids in the Chinese Altai: implications for Paleozoic tectonic evolution of the Central Asian Orogenic Belt. *Geoscience Frontiers* **9**, 1399–415.

Hoskin PWO and Schaltegger U (2003) The composition of zircon and igneous and metamorphic petrogenesis. *Reviews in Mineralogy and Geochemistry* **53**, 27–62.

Huang BC, Yan YG, Piper JDA, Zhang DH, Yi ZY, Yu S and Zhou TH (2018) Paleomagnetic constraints on the paleogeography of the East Asian blocks during Late Paleozoic and Early Mesozoic times. *Earth-Science Reviews* **186**, 8–36.

Huang BC, Yang ZY, Otofuji Y and Zhu RX (1999) Early Paleozoic paleomagnetic poles from the western part of the North China Block and their implications. *Tectonophysics* **308**, 377–402.

Hui J, Zhang KJ, Zhang J, Qu JF, Zhang BH, Zhao H and Niu PF (2021) Middle–late Permian high-K adakitic granitoids in the NE Alxa block, northern China: orogenic record following the closure of a Paleo-Asian oceanic branch? *Lithos* **400–401**, 106379. doi: 10.1016/j.lithos.2021.106379.

Irvine TH and Baragar WRA (1971) A guide to the chemical classification of the common volcanic rocks. *Canadian Journal of Earth Sciences* **8**, 523–48.

Jahn BM, Capdevila R, Liu DY, Vernon A and Badarch G (2004) Sources of Phanerozoic granitoids in the transect Bayanhongor-Ulaan Baatar, Mongolia: geochemical and Nd isotopic evidence, and implications for Phanerozoic crustal growth. *Journal of Asian Earth Sciences* **23**, 629–53.

Jian P, Liu D, Kröner A, Windley BF, Shi Y, Zhan F, Shi G, Miao L, Zhang W, Zhang Q, Zhang L and Ren J (2008) Time scale of an early to mid-Paleozoic orogenic cycle of the long-lived Central Asian Orogenic Belt, Inner Mongolia of China: implications for continental growth. *Lithos* **101**, 233–59.

Jian P, Liu D, Kröner A, Windley BF, Shi YR, Zhang W, Zhang FQ, Miao LC, Zhang LQ and Tomurhuu D (2010) Evolution of a Permian intra oceanic arc–trench system in the Solonker suture zone, Central Asian Orogenic Belt, China and Mongolia. *Lithos* **118**, 169–90.

Kemp AIS, Hawkesworth CJ, Foster GL, Paterson BA, Woodhead JD, Hergt JM, Gray CM and Whitehouse MJ (2007) Magmatic and crustal differentiation history of granitic rocks from Hf-O isotopes in zircon. *Science* **315**, 980–3.

Kemp T, Paterson B and Hawkesworth C (2005) A coupled Lu-Hf and O isotope in zircon approach to granite genesis. *Geochimica et Cosmochimica Acta* **69 (Suppl.)**, 243.

King PL, White AJR, Chappell BW and Allen CM (1997) Characterization and origin of aluminous A-type granites from the Lachlan Fold Belt, Southeastern Australia. *Journal of Petrology* **38**, 371–91.

Li S, Chung SL, Wilde SA, Jahn BM, Xiao WJ, Wang T and Guo QQ (2017) Early-Middle Triassic high Sr/Y granitoids in the southern Central Asian Orogenic Belt: implications for ocean closure in accretionary orogens. *Journal of Geophysical Research: Solid Earth* **122**, 2291–309.

Li S, Chung SL, Wilde SA, Wang T, Xiao WJ and Guo QQ (2016a) Linking magmatism with collision in an accretionary orogen. *Scientific Reports* **6**, 25751. doi: 10.1038/srep25751.

Li DP, Jin Y, Hou KJ, Chen YL and Lu Z (2015) Late Paleozoic final closure of the Paleo-Asian Ocean in the eastern part of the Xing-Meng Orogenic Belt: constrains from Carboniferous–Permian (meta-) sedimentary strata and (meta-) igneous rocks. *Tectonophysics* **665**, 251–62.

Li S, Wang T, Wilde SA and Tong Y (2013) Evolution, source and tectonic significance of Early Mesozoic granitoid magmatism in the Central Asian Orogenic Belt (central segment). *Earth-Science Reviews* **126**, 206–34.

Li S, Wang T, Wilde SA, Tong Y, Hong DW and Guo QQ (2012) Geochronology, petrogenesis and tectonic implications of Triassic granitoids from Beishan, NW China. *Lithos* **134–135**, 123–45.

Li S, Wilde SA, Wang T, Xiao WJ and Guo QQ (2016b) Latest Early Permian granitic magmatism in southern Inner Mongolia, China: implications for the tectonic evolution of the southeastern Central Asian Orogenic Belt. *Gondwana Research* **29**, 168–80.

Liu Y, Liu XM, Hu ZC, Diwu CR, Yuan HL and Gao S (2007) Evaluation of accuracy and long-term stability of determination of 37 trace elements in geological samples by ICP-MS. *Acta Petrologica Sinica* **23**, 1203–10 (in Chinese with English abstract).

Liu Q, Zhao G, Han Y, Eizenhöfer PR, Zhu YL, Hou WZ and Zhang XR (2017) Timing of the final closure of the Paleo-Asian Ocean in the Alxa Terrane: constraints from geochronology and geochemistry of Late Carboniferous to Permian gabbros and diorites. *Lithos* **274–275**, 19–30.

Liu Q, Zhao GC, Han YG, Li XP, Zhu YL, Eizenhöfer PR, Zhang XR, Wang B and Tsui RW (2018) Geochronology and geochemistry of Paleozoic to Mesozoic granitoids in Western Inner Mongolia, China: implications for the tectonic evolution of the Southern Central Asian Orogenic Belt. *Journal of Geology* **126**, 451–71.

Liu Q, Zhao GC, Han YG, Zhu YL, Wang B, Eizenhöfer PR and Zhang XR (2019a) Detrital zircon provenance constraints on the final closure of the middle segment of the Paleo-Asian Ocean. *Gondwana Research* **69**, 73–88.

https://doi.org/10.1017/S0016756822001157 Published online by Cambridge University Press

Liu Q, Zhao GC, Han YG, Zhu YL, Wang B, Eizenhöfer PR, Zhang XR and Tsui RW (2019b) Timing of the final closure of the middle segment of the Paleo-Asian Ocean: insights from geochronology and geochemistry of Carboniferous–Triassic volcanosedimentary successions in western Inner Mongolia, China. *Geological Society of America Bulletin* **131**, 941–65.

Liu Q, Zhao G, Sun M, Han YG, Eizenhöfer PR, Hou WZ, Zhang XR, Zhu YL, Wang B, Liu DX and Xu B (2016) Early Paleozoic subduction processes of the Paleo-Asian Ocean: insights from geochronology and geochemistry of Paleozoic plutons in the Alxa Terrane. *Lithos* **262**, 546–60.

Liu ZB and Zhang WJ (2014a) Geochemical characteristics and LA-ICP-MS zircon U-Pb dating of the Late Permian granodiorite in Hanggale, Alxa Right Banner, Inner Mongolia. *Geological Review* **60**, 409–26 (in Chinese with English abstract).

Liu ZB and Zhang WJ (2014b) Geochemical characteristics and LA-ICP-MS zircon U-Pb dating of Late Permian quartz monzodiorite in Hanggale, Inner Mongolia, China. *Journal of Chengdu University of Technology* **41**, 329–38 (in Chinese with English abstract).

Lu JC, Wei XY, Li YH and Wei JS (2012) Geochemical characteristics of Carboniferous-Permian hydrocarbon source rocks of Xiangtan 9 well in Ejin Banner, western Inner Mongolia. *Geological Bulletin of China* **31**, 1628–38 (in Chinese with English abstract).

Lu YH, Zhao ZF and Zheng YF (2016) Geochemical constraints on the source nature and melting conditions of Triassic granites from South Qinling in central China. *Lithos* **264**, 141–57.

Lu YH, Zhao ZF and Zheng YF (2017) Geochemical constraints on the nature of magma sources for Triassic granitoids from South Qinling in central China. *Lithos* **284–285**, 30–49.

Ludwig KR (2003) *User's Manual for Isoplot 3.00: A Geochronological Toolkit for Microsoft Excel*. Berkeley Geochronology Center, Special Publication no. 4.

Ma XH, Zhu WP, Zhou ZH and Qiao SL (2017) Transformation from Paleo-Asian Ocean closure to Paleo-Pacific subduction: new constraints from granitoids in the eastern Jilin-Heilongjiang Belt, NE China. *Journal of Asian Earth Sciences* **144**, 261–86.

Maniar PD and Piccoli PM (1989) Tectonic discrimination of granitoids. *Geological Society of America Bulletin* **101**, 635–43.

Martin H, Smithies RH, Rapp R, Moyen JF and Champion D (2005) An overview of adakite, tonalite–trondhjemite–granodiorite (TTG), and sanukitoid: relationships and some implications for crustal evolution. *Lithos* **79**, 1–24.

Meng E, Xu WL, Pei FP, Yang DB, Wang F and Zhang XZ (2011) Permian bimodal volcanism in the Zhangguangcai Range of eastern Heilongjiang Province, NE China: zircon U–Pb–Hf isotopes and geochemical evidence. *Journal of Asian Earth Sciences* **41**, 119–32.

Miller CF, McDowell SM and Mapes RW (2003) Hot and cold granites: implications of zircon saturation temperatures and preservation of inheritance. *Geology* **31**, 529–32.

Mushkin A, Navon O, Halica L, Hartmann G and Stein M (2003) The petrogenesis of A type magmas from the Amram Massif, Southern Israel. *Petrology* **44**, 815–32.

Niu YZ, Shi GR, Wang JQ, Liu CY, Zhou JL, Lu JC, Song B and Xu W (2021) The closing of the southern branch of the Paleo-Asian Ocean: constraints from sedimentary records in the southern Beishan Region of the Central Asian Orogenic Belt, NW China. *Marine and Petroleum Geology* **124**, 104791. doi: 10.1016/j.marpetgeo.2020.104791.

NXBG (Ningxia Bureau of Geology) (1980a) Geological Report of Wuliji. Ningxia Bureau of Geology (in Chinese).

NXBG (Ningxia Bureau of Geology) (1980b) Geological Report of Yingen. Ningxia Bureau of Geology (in Chinese).

NXBG (Ningxia Bureau of Geology) (1982) Geological Report of Shalataoerhan. Ningxia Bureau of Geology (in Chinese).

NXBG (Ningxia Bureau of Geology) (2001) Geological Report of Wuliji. Ningxia Bureau of Geology (in Chinese).

Patiño Douce AE (1999) What do experiments tell us about the relative contributions of crust and mantle to the origin of the granitic magmas? In *Understanding Granites: Integrating New and Classical Techniques* (eds A Castro, C Fernández and JL Vigneresse), pp. 55–75. Geological Society of London, Special Publication no. 168.

Pearce JA (1996) Sources and settings of granitic rocks. *Episodes* **19**, 120–5.

Pearce JA, Harris NBW and Tindle AG (1984) Trace element discrimination diagram for the tectonic interpretation of granitic rocks. *Journal of Petrology* **25**, 956–83.

Peccerillo A and Taylor AR (1976) Geochemistry of Eocene calc-alkaline volcanic rocks from the Kastamonu area, Northern Turkey. *Contributions to Mineralogy and Petrology* **58**, 63–81.

Pu JJ, Wu J, Duan XF, Jiang T, Shi JZ and Chen GC (2013) Permian brachiopod faunas from Engeerwusu Area in Yingen-Ejin Banner basin and its significance. *Geological Science and Technology Information* **32**, 1–5 (in Chinese with English abstract).

Quelhas P, Mata J and Dias Á (2020) Evidence for mixed contribution of mantle and lower and upper crust to the genesis of Jurassic I-type granites from Macao, SE China. *Geological Society of America Bulletin* **133**, 37–56.

Rapp RP and Watson EB (1995) Dehydration melting of metabasalt at 8–32 kbar: implications for continental growth and crust-mantle recycling. *Journal of Petrology* **36**, 891–931.

Rudnick RL and Fountain DM (1995) Nature and composition of the continental crust: a lower crustal perspective. *Reviews of Geophysics* **33**, 267–309.

Şengör AMC, Natal'in BA and Burtman VS (1993) Evolution of the Altaid tectonic collage and Palaeozoic crustal growth in Eurasia. *Nature* **364**, 299–307.

Shen XL, Du QX, Han ZZ, Song ZG, Han C, Zhong WJ and Ren X (2019) Constraints of zircon U-Pb-Hf isotopes from Late Permian-Middle Triassic flora-bearing strata in the Yanbian area (NE China) on a scissor-like closure model of the Paleo-Asian Ocean. *Journal of Asian Earth Sciences* **183**, 103964. doi: 10.1016/j.jseaes.2019.103964.

Shen P, Shen YC, Liu TB, Meng L, Dai HW and Yang YH (2009) Geochemical signature of porphyries in the Baogutu porphyry copper belt, western Junggar, NW China. *Gondwana Research* **16**, 227–42.

Shi XJ (2015) *The tectonic affinity of the Zongnaishan-Shalazhashan zone in northern Alxa and its implications: evidence from intrusive and metamorphic rocks*. Ph.D. thesis, Chinese Academy of Geological Sciences, Beijing, China. Published thesis.

Shi YR, Jian P, Kröner A, Li LL, Liu C and Zhang W (2016) Zircon ages and Hf isotopic compositions of Ordovician and Carboniferous granitoids from central Inner Mongolia and their significance for early and late Paleozoic evolution of the Central Asian Orogenic Belt. *Journal of Asian Earth Sciences* **117**, 153–69.

Shi GZ, Song GZ, Wang H, Huang CY, Zhang LD and Tang JR (2016) Late Paleozoic tectonics of the Solonker Zone in the Wuliji area, Inner Mongolia, China: insights from stratigraphic sequence, chronology, and sandstone geochemistry. *Journal of Asian Earth Sciences* **127**, 100–18.

Shi XJ, Tong Y, Wang T, Zhang JJ, Zhang ZC, Zhang L, Guo L, Zeng T and Geng JZ (2012) LA-ICP-MS zircon U–Pb age and geochemistry of the Early Permian Halinudeng granite in northern Alxa area, western Inner Mongolia. *Geological Bulletin of China* **31**, 662–70 (in Chinese with English abstract).

Shi XJ, Wang T, Zhang L, Castro A, Xiao XC, Tong Y, Zhang JJ, Guo L and Yang QD (2014a) Timing, petrogenesis and tectonic setting of the Late Paleozoic gabbro-granodiorite-granite intrusions in the Shalazhashan of northern Alxa: constraints on the southernmost boundary of the Central Asian Orogenic Belt. *Lithos* **208–209**, 158–77.

Shi XJ, Zhang L, Wang T, Xiao XC, Tong Y, Zhang JJ, Geng JZ and Ye K (2014b) Geochronology and geochemistry of the intermediate-acid intrusive rocks from Zongnaishan area in northern Alxa, Inner Mongolia, and their tectonic implications. *Acta Petrologica et Mineralogica* **33**, 989–1007 (in Chinese with English abstract).

Shi XJ, Zhang L, Wang T, Zhang JJ, Liu MH, Zhou HS and Yan YT (2016) Zircon geochronology and Hf isotopic compositions for the Mesoproterozoic gneisses in Zongnaishan area, northern Alxa and its tectonic affinity. *Acta Petrologica Sinica* **32**, 3518–36 (in Chinese with English abstract).

Song DF, Xiao WJ, Collins A, Glorie S and Han CM (2018a) Late Carboniferous-early Permian arc magmatism in the south-western Alxa Tectonic Belt (NW China): constraints on the late Palaeozoic subduction history of the Palaeo-Asian Ocean. *Geological Journal* **54**, 1046–63.

Song DF, Xiao WJ, Collins AS, Glorie S, Han CM and Li YC (2018b) Final subduction processes of the Paleo-Asian Ocean in the Alxa Tectonic Belt

(NW China): constraints from field and chronological data of Permian arc-related volcano-sedimentary rocks. *Tectonics* **37**, 1658–87.

Song DF, Xiao WJ, Windley BF and Han CM (2021) Provenance and tectonic setting of late Paleozoic sedimentary rocks from the Alxa Tectonic Belt (NW China): implications for accretionary tectonics of the southern Central Asian Orogenic Belt. *Geological Society of America Bulletin* **133**, 253–76.

Sun SS and McDonough WF (1989) Chemical and isotopic systematics of oceanic basalts: implications for mantle composition and processes. In *Magmatism in the Ocean Basins* (eds AD Saunders and MJ Norry), pp. 313–45. Geological Society of London, Special Publication no. 42.

Sylvester PJ (1998) Post-collisional strongly peraluminous granites. *Lithos* **45**, 29–44.

Tang K (1990) Tectonic development of Paleozoic fold belts at the north margin of the Sino-Korean Craton. *Tectonics* **9**, 249–60.

Taylor SR and McLennan SM (1985) The continental crust: its composition and evolution. An examination of the geochemical record preserved in sedimentary rocks. *Journal of Geology* **94**, 632–3.

Tian ZH, Xiao WJ, Windley BF, Zhang JE, Zhang ZY and Song DF (2017) Carboniferous rifted arcs leading to an archipelago of multiple arcs in the Beishan–Tianshan orogenic collages (NW China). *International Journal of Earth Sciences* **106**, 2319–42.

Topuz G, Candan O, Zack T, Chen F and Li QL (2019) Origin and significance of Early Miocene high-potassium I-type granite plutonism in the East Anatolian plateau (the Taşlıçay intrusion). *Lithos* **348–349**, 105210. doi: 10.1016/j.lithos.2019.105210.

Turner SP, Foden JD and Morrison RS (1992) Derivation of some A-type magmas by fractionation of basaltic magma—an example from the Padthaway Ridge, South Australia. *Lithos* **28**, 151–79.

Wang T, Tong Y, Zhang L, Li S, Huang H, Zhang JJ, Guo L, Yang QD, Hong DW, Donskaya T, Gladkochub D and Tserendash N (2017) Phanerozoic granitoids in the central and eastern parts of Central Asia and their tectonic significance. *Journal of Asian Earth Sciences* **145**, 368–92.

Wang ZJ, Xu WL, Pei FP, Wang ZW, Li Y and Cao HH (2015) Geochronology and geochemistry of middle Permian-Middle Triassic intrusive rocks from central-eastern Jilin Province, NE China: constraints on the tectonic evolution of the eastern segment of the Paleo-Asian Ocean. *Lithos* **238**, 13–25.

Wang TY, Wang SZ and Wang JR (1994) *The Formation and Evolution of Paleozoic Continental Crust in Alaxa Region*. Lanzhou: Lanzhou University Press (in Chinese with English abstract).

Watson EB and Harrison TM (1983) Zircon saturation revisited: temperature and composition effects in a variety of crustal magma types. *Earth and Planetary Science Letters* **64**, 295–304.

Whalen JB, Currie KL and Chappell BW (1987) A-type granites: geochemical characteristics, discrimination and petrogenesis. *Contributions to Mineralogy and Petrology* **95**, 407–41.

Wiedenbeck M, Alle P, Corfu F, Griffin WL, Meier M, Oberli F, von Quadt A, Roddick JC and Speigel W (1995) Three natural zircon standards for U-Th-Pb, Lu-Hf, trace and REE analyses. *Geostandards Newsletter* **19**, 1–23.

Wilhem C, Windley BF and Stampfli GM (2012) The Altaids of Central Asia: a tectonic and evolutionary innovative review. *Earth-Science Reviews* **13**, 303–41.

Wilson M (1989) *Igneous Petrogenesis*. London: Chapman & Hall, 466 pp.

Windley BF, Alexeiev D, Xiao WJ, Kröer A and Badarch G (2007) Tectonic models for accretion of the Central Asian Orogenic Belt. *Journal of the Geological Society, London* **164**, 31–47.

Wolf MB and Wyllie PJ (1994) Dehydration-melting of amphibolite at 10 kbar: the effects of temperature and time. *Contributions to Mineralogy and Petrology* **115**, 369–83.

Wu TR and He GQ (1992) Ophiolitic melange belts in the northern margin of the Alxa Block. *Geoscience* **6**, 286–96 (in Chinese with English abstract).

Wu TR and He GQ (1993) Tectonic units and their fundamental characteristics on the northern margin of the Alxa block. *Acta Geologica Sinica* **6**, 373–85.

Wu TR, He GQ and Zhang C (1998) On Palaeozoic tectonics in the Alxa Region, Inner Mongolia, China. *Acta Geologica Sinica* **72**, 256–63.

Wu FY, Li XH, Zheng YF and Gao S (2007) Lu-Hf isotopic systematics and their applications in petrology. *Acta Petrologica Sinica* **23**, 185–20 (in Chinese with English abstract).

Wu FY, Liu XC, Liu ZC, Wang RC, Xie L, Wang JM, Ji WQ, Yang L, Liu C, Khanal GP and He SX (2020) Highly fractionated Himalayan leucogranites and associated rare metal mineralization. *Lithos* **352–353**, 105319. doi: 10.1016/j.lithos.2019.105319.

Xiao WJ, Windley BF, Allen MB and Han CM (2013) Paleozoic multiple accretionary and collisional tectonics of the Chinese Tianshan orogenic collage. *Gondwana Research* **23**, 1316–41.

Xiao WJ, Windley BF, Han CM, Liu W, Wan B, Zhang JE, Ao SJ, Zhang ZY and Song DF (2018) Late Paleozoic to early Triassic multiple roll-back and oroclinal bending of the Mongolia collage in Central Asia. *Earth-Science Reviews* **186**, 94–128.

Xiao WJ, Windley BF, Huang BC, Han CM, Yuan C, Chen HL, Sun M, Sun S and Li JL (2009) End-Permian to mid-Triassic termination of the accretionary processes of the southern Altaids: implications for the geodynamic evolution, Phanerozoic continental growth, and metallogeny of Central Asia. *International Journal of Earth Sciences* **98**, 1189–287.

Xiao WJ, Windley B, Sun S, Li JL, Huang BC, Han CM, Yuan C, Sun M and Chen HL (2015) A tale of amalgamation of three Permo-Triassic collage systems in Central Asia: oroclines, sutures, and terminal accretion. *Annual Review of Earth and Planetary Sciences* **43**, 477–507.

Xie FQ, Wang LD, Li Q, Shi CX, Chen XB and Wei A (2015) Zircon LA-ICP-MS dating of granites from the Southeastern Zongnai Mountain Alax and its geochemical characteristics. *Rock and Mineral Analysis* **34**, 375–82 (in Chinese with English abstract).

Xie FQ, Wu JH, Sun YH, Wang LD, Wu JZ and Jia WJ (2021) Permian to Triassic tectonic evolution of the Alxa Tectonic Belt, NW China: constraints from petrogenesis and geochronology of felsic intrusions. *Lithos* **384–385**, 105980. doi: 10.1016/j.lithos.2021.105980.

Xie L, Yin HQ, Zhou HR and Zhang WJ (2014) Permian radiolarians from the Engeerwusu suture zone in Alxa area of Inner Mongolia and its geological significance. *Geological Bulletin of China* **33**, 691–7 (in Chinese with English abstract).

Xu B, Charvet J, Chen Y, Zhao P and Shi G (2013) Middle Paleozoic convergent orogenic belts in western Inner Mongolia (China): framework, kinematics, geochronology and implications for tectonic evolution of the Central Asian Orogenic Belt. *Gondwana Research* **23**, 1342–64.

Xu XY, Li RS, Chen JL, Ma ZP, Li ZP, Wang HL, Bai JK and Tang Z (2014) New constrains on the Paleozoic tectonic evolution of the northern Xinjiang area. *Acta Petrologica Sinica* **30**, 1521–34.

Xu DZ, Zhang WJ, Zhou HT and Sun QK (2014) Characteristics, zircon dating and tectonic significance of the gabbros along the north-central segments of the Alxa Block, Inner Mongolia. *Geological Bulletin of China* **33**, 661–71 (in Chinese with English abstract).

Yang QD, Zhang L, Wang T, Shi XJ, Zhang JJ, Tong Y, Guo L and Geng JZ (2014) Geochemistry and LA-ICP-MS zircon U-Pb age of Late Carboniferous Shalazhashan pluton on the northern margin of the Alxa Block, Inner Mongolia and their implications. *Geological Bulletin of China* **33**, 776–87 (in Chinese with English abstract).

Ye K, Zhang L, Wang T, Shi XJ, Zhang JJ and Liu C (2016) Geochronology, geochemistry and zircon Hf isotope of the Permian intermediate acid igneous rocks from the Yabulai Mountain in western Alxa, Inner Mongolia, and their tectonic implications. *Acta Petrologica et Mineralogica* **35**, 901–28 (in Chinese with English abstract).

Yin HQ, Zhou HR, Zhang WJ, Zheng XM and Wang SY (2016) Late Carboniferous to early Permian sedimentary–tectonic evolution of the north of Alxa, Inner Mongolia, China: evidence from the Amushan Formation. *Geoscience Frontiers* **7**, 733–41.

Yomeun BS, Wang W, Tchouankoue JP, Kamani MSK, Ndofack KIA, Huang SF, Basua EAA, Lu GM and Xue EK (2022) Petrogenesis and tectonic implication of Neoproterozoic I-type granitoids and orthogneisses in the Goa-Mandja area, Central African Fold Belt (Cameroon). *Lithos* **420-421**, 106700. doi: 10.1016/j.lithos.2022.106700.

Zhang SH (2019) *Geological characteristics and later reformation of the Permo-Carboniferous basin in Yingen-Ejina area, NW China*. Ph.D. thesis, Northwest University, Xi'an, China. Published thesis.

Zhang DH, Huang B, Zhao J, Meert JG, Zhang Y, Liang YL, Bai QH and Zhou TH (2018) Permian paleogeography of the Eastern CAOB:

https://doi.org/10.1017/S0016756822001157 Published online by Cambridge University Press

paleomagnetic constraints from volcanic rocks in Central Eastern Inner Mongolia, NE China. *Journal of Geophysical Research: Solid Earth* **123**, 2559–82.

Zhang ZP, Liu G, Xu C, Meng QT and Guo C (2016) Geochemical characteristics and LA-ICP-MS zircon U-Pb dating of the Late Permian granites in the Tamusu area of Alxa Right Banner, Inner Mongolia and their implications. *Geology and Exploration* **52**, 893–909 (in Chinese with English abstract).

Zhang W, Pease V, Meng QP, Zheng RG, Thomsen TB, Wohlgemuth-Ueberwasser C and Wu TR (2015) Timing, petrogenesis, and setting of granites from the southern Beishan late Palaeozoic granitic belt, Northwest China and implications for their tectonic evolution. *International Geology Review* **57**, 1975–91.

Zhang W, Pease V, Meng QP, Zheng RG, Thomsen TB, Wohlgemuth-Ueberwasser C and Wu TR (2016) Discovery of a Neoproterozoic granite in the northern Alxa region, NW China: its age, petrogenesis and tectonic significance. *Geological Magazine* **153**, 512–23.

Zhang W, Pease V, Meng QP, Zheng RG, Wu TR, Chen Y and Gan LS (2017) Age and petrogenesis of late Paleozoic granites from the northernmost Alxa region, Northwest China, and implications for the tectonic evolution of the region. *International Journal of Earth Sciences* **106**, 79–96.

Zhang JJ, Wang T, Zhang L, Tong Y, Zhang ZC, Shi XJ, Guo L, Huang H, Yang QD, Huang W, Zhao JX, Ye K and Hou JY (2015) Tracking deep crust by zircon xenocrysts within igneous rocks from the northern Alxa, China: constraints on the southern boundary of the Central Asian Orogenic Belt. *Journal of Asian Earth Sciences* **108**, 150–69.

Zhang W, Wu TR, Feng JC, Zheng RG and He YK (2013) Time constraints for the closing of the Paleo-Asian Ocean in the Northern Alxa Region: evidence from Wuliji granites. *Science China Earth Sciences* **56**, 153–64.

Zhang YQ and Zhang T (2016) Amushan Formation in Inner Mongolia. *Geology in China* **43**, 1000–15 (in Chinese with English abstract).

Zhang XR, Zhao GC, Eizenhöfer PR, Sun M, Han YG, Hou WZ, Liu DX, Wang B, Liu Q and Xu B (2015a) Paleozoic magmatism and metamorphism in the Central Tianshan block revealed by U-Pb and Lu-Hf isotope studies of detrital zircons from the South Tianshan belt, NW China. *Lithos* **233**, 193–208.

Zhang XR, Zhao GC, Eizenhöfer PR, Sun M, Han YG, Hou WZ, Liu DX, Wang B, Liu Q and Xu B (2015b) Latest Carboniferous closure of the Junggar Ocean constrained by geochemical and zircon U-Pb-Hf isotopic data of granitic gneisses from the Central Tianshan block, NW China. *Lithos* **238**, 26–36.

Zhang Z, Zhou G, Kusky TM, Yan S, Chen B and Zhao L (2009) Late Paleozoic volcanic record of the Eastern Junggar terrane, Xinjiang, Northwestern China: major and trace element characteristics, Sr-Nd isotopic systematics and implications for tectonic evolution. *Gondwana Research* **16**, 201–15.

Zhao ZL, Li JJ, Dang ZC, Tang WL, Fu C, Wang SG, Liu LS, Zhao LJ and Liu XX (2016) TIMS zircon U-Pb isotopic dating of Salazha Mountain granites from the North Margin of Alxa, Inner Mongolia, and its tectonic implications. *Geological Bulletin of China* **35**, 599–604 (in Chinese with English abstract).

Zhao YL, Li W, Wen QB, Liang CY, Feng ZQ, Zhou JP and Shen L (2016) Late Paleozoic tectonic framework of eastern Inner Mongolia: evidence from the detrital zircon U–Pb ages of the Mid-late Permian to Early Triassic sandstones. *Acta Petrologica Sinica* **32**, 2807–22 (in Chinese with English abstract).

Zhao XC, Liu CY, Wang JQ, Zhang SH and Guan YZ (2020) Geochemistry, geochronology and Hf isotope of granitoids in the northern Alxa region: implications for the Late Paleozoic tectonic evolution of the Central Asian Orogenic Belt. *Geoscience Frontiers* **11**, 1711–25.

Zhao Y, Sun Y, Diwu CR, Zhu T, Ao WH, Zhang H and Yan JH (2017) Paleozoic intrusive rocks from the Dunhuang tectonic belt, NW China: constraints on the tectonic evolution of the southernmost Central Asian Orogenic Belt. *Journal of Asian Earth Sciences* **138**, 562–87.

Zhao GC, Wang YJ, Huang BC, Dong YP, Li SZ, Zhang GW and Yu S (2018) Geological reconstructions of the East Asian blocks: from the breakup of Rodinia to the assembly of Pangea. *Earth-Science Reviews* **186**, 262–86.

Zhao P, Xu B and Zhang C (2017) A rift system in southeastern Central Asian Orogenic Belt: constraint from sedimentological, geochronological and geochemical investigations of the Late Carboniferous-Early Permian strata in northern Inner Mongolia (China). *Gondwana Research* **47**, 342–57.

Zheng B, Han BF, Liu B and Wang ZZ (2019) Ediacaran to Paleozoic magmatism in West Junggar Orogenic Belt, NW China, and implications for evolution of Central Asian Orogenic Belt. *Lithos* **338–339**, 111–27.

Zheng RG, Li JY, Xiao WJ, Liu JF and Wu TR (2016) Discovery of Silurian pluton in the Enger Us region in the northern margin of Alxa Block. *Acta Geologica Sinica* **80**, 1725–36 (in Chinese with English abstract).

Zheng RG, Wu TR, Zhang W, Xu C, Meng QP and Zhang ZY (2014) Late Paleozoic subduction system in the northern margin of the Alxa block, Altaids: geochronological and geochemical evidences from ophiolites. *Gondwana Research* **25**, 842–58.

Zhu RZ, Lai SC, Qin JF and Zhao SW (2018) Petrogenesis of late Paleozoic-to-early Mesozoic granitoids and metagabbroic rocks of the Tengchong block, SW China: implications for the evolution of the eastern paleo-Tethys. *International Journal of Earth Sciences* **107**, 431–82.

Zhu Y, Lai SC, Qin JF, Zhu RZ, Zhang FY and Zhang ZZ (2018) Geochemistry and zircon U–Pb–Hf isotopes of the 780 Ma I-type granites in the western Yangtze Block: petrogenesis and crustal evolution. *International Geology Review* **61**, 1222–43.

https://doi.org/10.1017/S0016756822001157 Published online by Cambridge University Press